phys. stat. sol. (a) **162**, 5 (1997)

Subject classification: 78.40.Fy; 71.35.Ee; 71.35.Gg; 71.55.Ht; 78.55.Mb; S6

Optical Characterization of Silicon Carbide Polytypes

R. P. Devaty and W. J. Choyke

Department of Physics and Astronomy, University of Pittsburgh, Pittsburgh, PA 15260, USA

(Received January 31, 1997)

This article is a review of recent progress in our understanding of the optical properties of the important polytypes of SiC: 3C, 4H, 6H, and 15R. We focus on experimental work but also compare results obtained by experiment with theory. The topics of emphasis are: 1. vacuum ultraviolet reflectivity, 2. free excitons, 3. spectroscopy of shallow donors and acceptors, 4. the impurity boron in SiC, 5. the rare earth impurity erbium in SiC, and 6. optical properties of porous SiC.

1. Introduction

Continued progress in the development of SiC as a high temperature, high power, high speed, radiation resistant device material depends on improving the state of the underlying knowledge base required for device modeling, materials characterization and diagnostics. Much of what is presently known has been acquired over five decades by optical techniques. The purpose of this article is to review recent progress in optical studies of the important polytypes of SiC, to point out some of the many gaps in our knowledge, and to provide background to the literature. The topics selected for emphasis are vacuum ultraviolet reflectivity, free excitons, shallow donors and acceptors, boron in SiC, erbium in SiC, and porous SiC. Many topics have been omitted, including transition metal impurities, defects and radiation damage, and hydrogen in SiC. Further information is available in earlier reviews [1 to 8].

2. Ultraviolet Reflectivity and Band Structure of SiC Polytypes

Detailed knowledge of the electronic energy band structure and wave functions for the important SiC polytypes is an essential ingredient for the development of accurate, reliable models of impurity and defect states, scattering processes, and transport coefficients required for device modeling. Optical reflectivity of SiC, particularly in the near and middle ultraviolet (4 to 11 eV), provides a test for the qualitative reliability of calculations. Although measurements of the optical reflectivity of SiC [9 to 12] have been performed and compared with calculated band structures [13 to 19] since the 1960s, recent advances in both materials quality and first principles calculations have led to a fruitful reawakening of this field in the 1990s. Excellent large area as-grown surfaces for the measurement of the vacuum ultraviolet (uv) reflectivity are now available as homoepitaxial layers grown on boule substrates of 4H, 6H, and 15R SiC and epitaxial layers of 3C SiC grown on 6H SiC boule wafers as well as on 3C SiC bulk crystals. Increased

sophistication made possible by advances in computing power coupled with better understanding of the underlying approximations have led to improved calculations based on first principles that may be performed for polytypes having large unit cells. A close collaboration between the experimental and theoretical efforts makes possible a detailed interpretation of measured spectra and a strong test of theory which may lead to further improvements.

Lambrecht et al. [20, 21] performed such a study using a reflectometer described by Suttrop et al. [22] covering the 4 to 10 eV region. Room temperature spectra were recorded for 3C, 6H, 15R, and 4H SiC, while the reflectivity was calculated for 3C, 6H, 4H, and 2H SiC, allowing a consideration of trends among polytypes versus hexagonality. The accuracy of absolute reflectance measurements obtainable with the present apparatus and samples is at best about 10%. For purposes of comparison, the spectra reported in [21] were multiplicatively normalized so that the reflectivity at 4.0 eV agrees with the value $R = 0.204$ obtained using the index of refraction $n = 2.65$. Based on a fit to the measured energy dependence of the index [23], the extrapolated value at 4.0 eV is $n = 2.95$, leading to $R = 0.244$. Thus, the reflectivities in [21] are seemingly too low. Logothetidis et al. [24, 25] have also discussed the index of refraction.

While many features in the measured reflectivity of 3C SiC may be interpreted using calculated critical point transitions at symmetry points in the Brillouin zone, an important result of this new work is that the major peaks in the reflectivity are associated with rather extended regions of **k**-space over which the energy difference between two bands is nearly constant. These regions are identified by examining the **k**-space dependence of each band-to-band contribution separately. An adjustment (scissors operator shift) of 1.00 eV to the calculated spectra, independent of energy, wavevector and polytype, leads to tenths of an eV agreement in the energy positions of measured and calculated features, indicating that these calculations performed in the Local Density Approximation (LDA) are accurate to this level after correction for this well-known underestimate of the band gaps. Adolph et al. [26, 27], Gavrilenko and Bechstedt [28] and Wenzien et al. [29] examined corrections to the LDA and provide some comparison with experiment. While a scissors operator shift is satisfactory for the calculated dielectric function and reflectivity over the 1 to 10 eV range, the calculated overall shift exceeds the value required for agreement with experiment. In addition, the quasiparticle energy shifts do in fact depend significantly on **k** and band index. Rohlfing et al. [30] and Backes et al. [31] have also considered quasiparticle energy shifts for the 3C SiC band structure. Lambrecht et al. [32] discuss calculations of the uv reflectivity in detail elsewhere in this volume.

To complete the survey of recent work in the uv, we cite the studies of Gavrilenko et al. on 3C [33] and 4H SiC [34] by electroreflectance, the calculations of the differential reflectance of the (110) surface of 3C SiC by Gavrilenko [35], and the measurements by Logothetidis et al. [24, 25] on 3C and 6H SiC by spectroscopic ellipsometry using synchrotron radiation.

The calculated reflectivity spectra for the hexagonal and rhombohedral polytypes show considerable anisotropy. Adolph et al. [36] recently calculated the normal incidence uv reflectivity of 4H and 6H SiC for polarizations $\mathbf{E} \perp \mathbf{c}$ and $\mathbf{E} \parallel \mathbf{c}$. Lambrecht et al. [32] calculated the uv reflectivity out to 25 eV for 2H, 4H, 15R, 6H, and 3C SiC. Theory may be tested by measuring the reflectivity for both polarizations, using large area (greater than one-inch diameter) *a*-face and prism face samples when they become avail-

able. Such measurements are best performed taking advantage of the high intensity beam available from a synchrotron. Use of modulation spectroscopy will enhance fine structure in the spectra.

3. Free Excitons

Free Wannier excitons in semiconductors can be treated theoretically using effective mass theory [37 to 39]. For a simple two-band model (nondegenerate isotropic parabolic bands) of a direct gap semiconductor, the Hamiltonian, originally written in terms of the dynamical variables of the electron and hole, can be rewritten in terms of variables associated with center of mass and relative motions. The wave function for the relative motion is the product of an envelope wave function, obtained by solving the effective mass equation, and the Bloch functions at the valence band maximum and conduction band minimum. The energy level structure of the exciton is hydrogen-like if the valence and conduction bands are assumed isotropic and parabolic. For an indirect gap semiconductor such as one of the polytypes of SiC, there are additional considerations: 1. orbital degeneracy at the valence band maximum for 3C SiC; 2. closely spaced valence bands relative to the exciton binding energy for all polytypes, due to the small spin−orbit splitting; 3. anisotropic conduction band minima, which lead to valley anisotropy induced splittings, and 4. possible small splittings due to the electron−hole exchange interaction. Consider 3C SiC as an example. Neglecting spin, the valence band maximum is an orbital triplet at the point Γ and the conduction band minimum is a singlet at X. The free exciton wave function is composed of products of the Bloch functions at the valence band maximum and conduction band minimum as well as an envelope function. Since the electron is part of the exciton, there is a reduction of symmetry (related to the anisotropy of the conduction electron valley) leading to an anisotropy splitting of the exciton. Assuming that the envelope function is a completely symmetric singlet, the threefold degeneracy would undergo a valley anisotropy induced splitting into a singlet and a doublet. Inclusion of electron spin increases the number of states under consideration to twelve, with additional splittings due to the exchange part of the Coulomb interaction between electron and hole. Therefore, based on symmetry considerations, the twelve states split into six doublets. According to an interpretation of far infrared absorption data [40] for silicon, the anisotropy and exchange splittings for the free exciton are comparable in magnitude.

McLean and Loudon [41] used a variational method to calculate the exciton binding energies for silicon and germanium. Details of the structure of the valence bands and anisotropy of the conduction band near the minimum were included, but the electron−hole exchange coupling was neglected. Lipari and Altarelli [42, 43] introduced an approximation method based on analysis of terms of the exciton Hamiltonian classified by symmetries and used it to calculate the binding energies and excited states of indirect excitons in Si, Ge, GaP, and AlSb. Their results are generally consistent with measured features in the absorption spectra of these semiconductors, as discussed in [42, 43]. Electron−hole exchange coupling was neglected. This method was applied to 3C SiC by Bimberg et al. [44], who obtained a binding energy of 26.7 meV for the free exciton, which is the presently accepted value. The success of this method depends on knowledge of the valence and conduction band effective mass parameters. To the best of our knowledge there are no reliable calculated values for the free exciton binding energies in any

other SiC polytype. Detailed far infrared absorption spectra of free excitons in silicon [40] were interpreted in terms of a different model based on donor-like states, so there is still some question regarding the best model to interpret fine structure in free exciton spectra.

Radiative recombination of a free exciton in a perfect crystal must be accompanied by creation or destruction of at least one phonon to conserve crystal momentum. The group theoretical methods for the determination of selection rules for indirect transitions are discussed in detail by Elliott and Loudon [45] and Lax and Hopfield [46]. Selection rules for indirect excitons have been discussed for 3C SiC [47, 48] and 6H SiC [49] (assuming that the conduction band minimum for 6H SiC is at M rather than at a point U on the M–L line). Due to the conservation laws, free exciton lines can be quite sharp, especially at low temperatures, and analysis of details of the lineshapes might reveal fine structure in the exciton levels as well as the temperature of the exciton gas.

The electron–hole liquid (EHL) has been observed in 3C [50, 51], 15R [52] and 4H SiC [52]. The high value for the critical temperature of about 41 K determined for 3C SiC is consistent with a large binding energy for the free exciton. An argument [52] based on the high density of the EHL in 15R SiC indicates that the critical temperature exceeds 60 K.

Free excitons play an essential role in the detailed energy dependence of the fundamental absorption spectrum in SiC polytypes. Elliott [53] discussed the energy dependence of the absorption edge of an indirect semiconductor. The absorption edge was measured in 6H [54], 4H [55], 3C [56], 15R [57], 21R [58], 33R [59] and 2H SiC [60], leading to a clear identification of all these polytypes as indirect semiconductors and a determinationn of the temperature dependence of the exciton gap. The measured energies of phonons emitted at low temperatures to conserve crystal momentum in the absorption process, while not as precise, were consistent with the phonon energies obtained using the recombination of neutral four-particle nitrogen donor (bound exciton) complexes measured by low temperature photoluminescence (LTPL). The recombination of free excitons is observed in luminescence for samples of sufficient quality and purity. Recombination of intrinsic excitons was first reported in 6H [54] and 4H SiC [55]. Nedzvetskii et al. [61] studied free excitons in 3C SiC by both absorption and photoluminescence. Pikhtin and Yaskov [62] measured the fundamental absorption edge of 6H SiC from 4.2 to 600 K, enabling them to observe transitions assisted by phonon absorption as well as emission. Modulated absorption spectroscopy can enhance fine structure in the absorption spectrum, thus revealing details of the electronic structure of free excitons, but great care must be taken both in the experimental technique and interpretation [63].

Free exciton spectra contain information about valence band structure in addition to information about the free excitons themselves. Theorists are just beginning to calculate the detailed structure near the top of the valence bands for the important SiC polytypes [32, 64, 64a]. Analysis of free exciton spectra can provide measured values for the spin–orbit and crystal field splittings. Due to the difficulty of the experiments and their interpretation, reliable measured values of the crystal field splittings of the valence bands for the hexagonal and rhombohedral polytypes do not exist, although there are some values reported in the literature for 6H [65, 66] and 4H SiC [67] obtained by electroabsorption spectroscopy. Measured values of the spin–orbit splitting of the valence bands are reliable, with the caveat that there is a small difference between a value measured using

free excitons and the value for free holes. According to the calculations of Bimberg et al. [44] this difference is about 0.2 meV. Humphreys et al. [68, 69] measured the wavelength modulated absorption spectrum of 3C, 6H, and 15R SiC and obtained 10 meV for 3C SiC and 7 meV for 6H and 15R SiC for the spin–orbit splitting of the valence bands. Gorban et al. [47] measured absorption, wavelength modulated absorption, and photoluminescence spectra of 3C SiC at 1.2 K. They interpreted fine structure in their spectra to obtain the value (10.36 ± 0.03) meV for the spin–orbit splitting and (0.59 ± 0.03) meV for the valley anisotropy splitting of the 1s ground state multiplet of the indirect exciton. Bimberg et al. [44] calculated 0.8 meV for the anisotropy splitting.

There are no reliable measured values for the binding energy of free excitons in any SiC polytype. As an example of the unreliability of interpretation of subtle spectral features, Kiselev et al. [70] estimated $E_X = 14$ meV for 3C SiC based on a change in the power law energy dependence of the absorption coefficient measured at 4.2 K, in substantial disagreement with the presently accepted value of 27 meV [44]. Sankin [66] analyzed the 2 K electroabsorption spectra of 6H SiC measured for both $\mathbf{E} \parallel \mathbf{c}$ and $\mathbf{E} \perp \mathbf{c}$ to estimate the value $E_X = 78$ meV. By the same method, Dubrovskii and Sankin [67] obtained $E_X = 20$ meV for 4H SiC. In both cases, even if the identification of features in their complex spectra is correct, the values for E_X are estimates based on the hydrogenic model for a free exciton. Ikeda and Matsunami [71] determined the activation energies for thermal quenching of free excitons through study of the temperature dependence of the free exciton luminescence. Their values of 7, 10, 29, and 20 meV for 3C, 4H, 6H, and 15R SiC, respectively, are too small to be regarded as the free exciton binding energies.

It is clear that there is a need for both experimental and theoretical work on the electronic structure of free excitons in SiC polytypes. Knowledge of the binding energies is especially important to obtain the indirect band gap $E_G = E_{GX} + E_X$ needed to obtain accurate impurity binding energies from donor–acceptor pair and free to bound luminescence spectra.

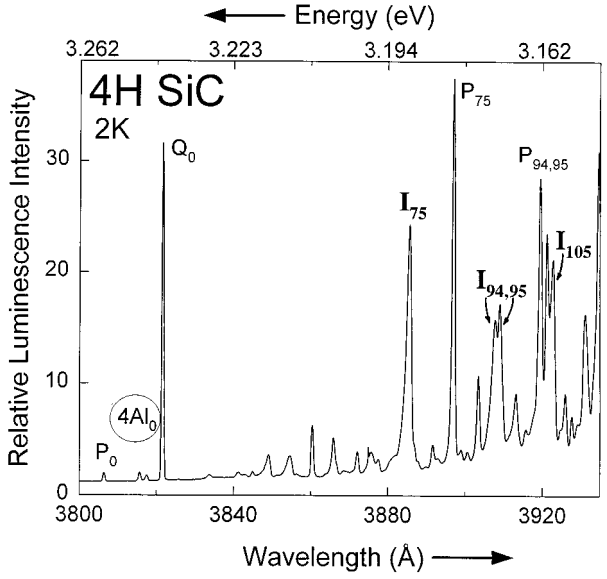

Fig. 1. Low temperature photoluminescence spectrum of a single crystal 4H SiC epilayer grown by CVD on a 4H SiC substrate. Strong free exciton lines are labeled I. Lines P and Q are due to the neutral nitrogen donor four-particle bound exciton complex. Lines $4Al_0$ are no-phonon lines of the neutral aluminum acceptor four-particle complex. In all cases the subscript indicates the energy of the participating momentum conserving phonon in meV

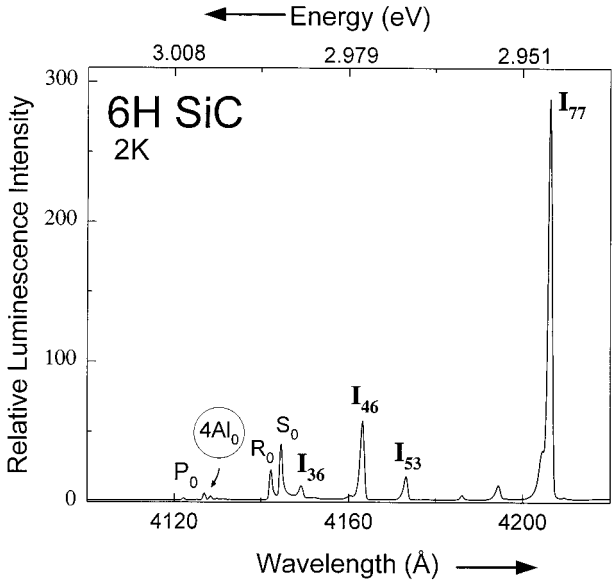

Fig. 2. Low temperature photoluminescence spectrum of a single crystal 6H SiC epilayer grown by CVD on a 6H SiC substrate. Strong free exciton lines are labeled I. The subscripts indicate the energies of participating momentum conserving phonons in meV. P_0, R_0 and S_0 are no-phonon lines of the neutral nitrogen donor four-particle bound exciton complex. $4Al_0$ labels the no-phonon spectrum of the neutral aluminum four-particle complex

Free exciton low temperature luminescence spectra in high quality single crystal films of 4H and 6H SiC have been observed in the last few years by a number of groups [72 to 75]. Fig. 1 and 2 show strong free exciton spectra in CVD grown homoepitaxial 4H and 6H SiC films recorded in our laboratory. Kordina et al. observed free exciton lines in thick films of 6H [72, 73] and 4H SiC [74] grown in a hot-wall CVD reactor.

4. Shallow Donors

Effective mass theory [76 to 78] provides the basis for understanding the electronic structure of shallow donors in semiconductors. The parameters of this theory are the elements of the electron effective mass tensor at the minimum of the lowest conduction band and the static dielectric tensor. If one knows these parameters, one may use effective mass theory to calculate the energy levels of a shallow donor. Otherwise, one may determine the parameters by adjusting them to fit the theory to a measured spectrum.

The elements of the static dielectric tensor have been measured in 3C [79, 80] and 6H SiC [79]. Recently, calculations of the static dielectric tensor for 3C, 2H and 4H SiC have been performed [81, 82]. Electron effective masses have been calculated [29, 64, 83 to 86] for 3C, 2H, 4H, 6H, and 15R SiC. The values of the effective masses, which describe curvatures in the bands, are determined in part by the energy separations of nearby bands. If the masses are known from experiment, their values provide a test of the ability of a calculation to accurately describe the real material. Because the Local Density Approximation (LDA) leads to a well-known underestimate of energy gaps, one might expect disagreement with measured effective masses due to the incorrect spacings of bands. Experimentally, our knowledge of the electron effective masses of the important SiC polytypes, listed in Table 1, is incomplete. The electron effective masses for 3C SiC, for which the conduction band minimum is at (or very near) the X point of the Brillouin zone, are the most reliably known, since the measured values obtained by three independent techniques – two-electron transitions in low temperature photolumines-

Table 1
Measured conduction band effective masses, relative to the bare electron mass, in silicon carbide polytypes

polytype	location of minimum	effective masses	ref.
3C	X	$m_t = 0.247 \pm 0.011$ $m_l = 0.677 \pm 0.015$	[87, 88]
4H	M	$m_{M\Gamma} = 0.58 \pm 0.01$ $m_{MK} = 0.31 \pm 0.01$ $m_{ML} = 0.33 \pm 0.01$	[83]
6H	U	$m_\perp = (m_{M\Gamma} m_{MK})^{1/2} = 0.42 \pm 0.2$ $m_{ML} = 2.0 \pm 0.2$	[96]

cence spectra [87], far infrared cyclotron resonance [88], and infrared absorption by nitrogen donors [89 to 91] – are in agreement. A camel's back at X would lead to a nonlinear dependence of the cyclotron resonance frequency on the applied magnetic field. Electron effective masses obtained by cyclotron resonance at fields up to 150 T [92 to 94] are unchanged from values measured at lower fields, providing evidence that the conduction band minimum is very close to X. Theory and experiment now indicate consistently that the conduction band minima of 4H SiC are at the M points of the hexagonal Brillouin zone. Thus, there are three equivalent minima. Values for the three diagonal components of the electron effective mass tensor in 4H SiC obtained by optical detection of cyclotron resonance (ODCR) [83, 95] are consistent with calculated values [64, 83, 84]. ODCR has also been performed on 6H SiC [96], but the two effective masses perpendicular to the *c*-axis have not been resolved. The mass component parallel to the M–L axis may depend significantly on the filling of a nonparabolic double well-like conduction band near the minimum [84]. For 15R SiC, the locations of the conduction band minima have been calculated and effective masses obtained [86], but there is no reliable set of measured mass parameters available for comparison.

Effective Mass Theory (EMT) is based on the assumption of Coulomb attraction between the extra electron and the donor impurity ion, and does not include any information concerning the specific impurity. It usually underestimates the binding energy of the ground state and to a lesser extent excited states due to neglect of "central cell effects" associated with the change in the potential introduced by the substitutional impurity. The effect of the central cell potential on p-states is minimal because the electron wave function has a node at the impurity site. Since all the important SiC polytypes are indirect semiconductors and have multiple conduction band minima, a further consequence of corrections to EMT is the possible reduction of degeneracy in the ground state due to valley–orbit splitting. Because even shallow donors in SiC are relatively tightly bound, the envelope wave function of the bound electron may not uniformly sample the complex unit cell of a polytype such as 6H or 15R SiC. Although the impurity central cell potential may be the same, the binding energies are site dependent. Thus, a donor such as nitrogen substituting on a carbon site in 6H SiC is in fact three different donors with different sets of electronic energy levels because there are three inequivalent carbon sites with distinct local environments, one hexagonal (h) and two quasicubic (k_1 and k_2) with respect to next nearest neighbors. The Kohn-Luttinger inter-

ference effect [77, 97] plays a role in determining these differences. The calculation of reliable energy levels and the detailed explanation of the physical origins of the site dependence are challenges to the theory of shallow donors, especially since each polytype has a different band structure.

Because SiC is a binary semiconductor, it is possible for an impurity to substitute on either the carbon or silicon sublattice. Although there may be reasons for an impurity to strongly favor one of the sublattices such as size and electronegativity, control of growth conditions may tip the balance via the mechanism of site competition epitaxy [98 to 100]. The electronic structure of an impurity substituting on a carbon site may be quite different from a silicon site. The situation is most clear for 3C SiC. The conduction band minimum is located at (or very near) the point X in the Brillouin zone. As Morgan [101] discussed, the symmetry label of the electron wave function at the minimum depends on the choice of origin. An X_1 wave function (neglecting electron spin) is even (in the coordinate x, say, along the direction k_x associated with the minimum under consideration), whereas an X_3 Bloch function is odd. In treating the problem of a substitutional impurity, one chooses the origin at the impurity site. For a donor substituting on a carbon site the X_1 label applies, indicating that electron density tends to pile up on the carbon atoms. Given the symmetry of the Bloch function at the conduction band minimum, the T_d local symmetry of the substitutional impurity implies a valley–orbit splitting of the threefold degeneracy associated with the three equivalent conduction band minima into a singlet and a doublet. The symmetric singlet state is lower in energy and therefore the ground state of the impurity. If the donor substitutes rather on a silicon site, the Bloch functions at the minima are p-like with respect to the origin. There is no valley–orbit splitting so that the ground state is a triplet. If spin is included, there is a small spin–valley splitting into a doublet and quadruplet. Larkin [100] discussed the possibility of introducing nitrogen preferentially into silicon sites by site competition epitaxy. No optical signature for silicon site nitrogen has been identified in any SiC polytype.

5. Nitrogen Donors

Biedermann [102] observed strongly polarized absorption bands in the visible and near infrared in 4H, 6H, 8H, and 15R SiC heavily doped with nitrogen. These bands are presently interpreted as due to direct transitions from initial states near the lowest conduction band minimum or nitrogen donor levels to higher conduction bands. Dubrovskii et al. [103] included 21R, 27R, and 33R SiC in their study of seven polytypes at several temperatures. Gorban et al. [104] investigated the temperature dependence of these bands in 4H SiC as a probe of the electronic structure of the nitrogen donors. They determined values of 57 meV and less than 10 meV for the valley–orbit splittings of nitrogen on k and h sites, respectively, and estimated the binding energy of k-site nitrogen as 113 meV using the value of 66 meV for the h site [105]. A comparison of the absorption spectra with state of the art calculated band structures should lead to the identification of the transitions as well as test ability of first principles theory to describe the actual materials.

In low temperature photoluminescence (LTPL), the presence of nitrogen is indicated by the 4N spectrum associated with the radiative recombination of a neutral four-particle (bound exciton) Lampert [106] complex. The four particles making up the complex are the donor ion, two electrons, and a hole. Since the electrons are indistinguishable

and typically occupy degenerate single particle states with antiparallel spins, an exciton loses its distinct identity when it becomes attached to a donor. The final state is a neutral donor, usually in its ground state. Because SiC is an indirect semiconductor, most of the radiative recombination is accompanied by phonon emission. Lines associated with momentum conserving (MC) phonons are observed, indicating that the electron wave function is localized in **k**-space. The MC phonons provide information regarding the **k**-space location of the conduction band minima. Hofmann et al. [107] calculated phonon dispersion relations for 3C, 6H, 4H, and 2H SiC using a phenomenological bond charge model. Lambrecht et al. [108] compared the calculated frequencies with the MC phonon replicas of 4N for 4H and 6H SiC measured by the Westinghouse group [54 to 55]. Choyke et al. [109] carefully examined LTPL 4N spectra of 4H and 6H SiC and compared the measured frequencies of MC phonons with calculated values [107] for points along the M–U–L line in the Brillouin zone. For 4H SiC, the comparison supports the location of the conduction band minima at the M points. For 6H SiC, the comparison is inconclusive in deciding between the M point and the point U associated with the calculated location of the minimum, although the L point is eliminated. There is strong support based on both theory and experiment that the minimum is at a U point. A possible location for this U point was calculated by Lambrecht et al. [108]. The strong polarization of MC phonon lines parallel or perpendicular to the crystal *c*-axis observed for hexagonal polytypes has not been used in comparisons with theory.

Due to the loss of translational invariance associated with the binding of the exciton, sharp no-phonon lines are observed in 4N spectra by LTPL. The strength of the no-phonon line relative to the MC replicas tends to increase with the exciton binding energy to the impurity. For 3C SiC [56] and the hexagonal polytypes 2H [60], 4H [55], and 6H SiC [54], the number of no-phonon lines is equal to the number of inequivalent sites on the C sublattice. However, for the rhombohedral polytypes 15R [57], 21R [58], and 33R SiC [59], for reasons unknown, the number of observed no-phonon lines is one less than the number of inequivalent sites. As the temperature is raised, excited states are observed. For 6H [54], 15R [57], 21R [58] and 33R SiC [59] excited states 4.8 meV above the no-phonon lines were identified as 4N complexes with the hole taken from the next valence band split off by the small spin–orbit interaction. The energy 4.8 meV is not to be regarded as a precise value for the spin–orbit splitting of the valence band. The fact that the same value is measured for several polytypes is taken as evidence that the valence band structure is similar for these polytypes. For 2H SiC [60], the complex is too weakly bound to observe this splitting by raising the temperature, but an observed state 5 meV below the no-phonon line is attributed to a transition for which the neutral nitrogen donor is left in the upper valley–orbit state. For 3C SiC [56], excited states are observed 2 and 5 meV above the no-phonon line at 15 K, but not identified with certainty.

Application of a symmetry-reducing perturbation can provide important clues to the electronic structure of a four-particle complex. Hartman and Dean [110] performed magneto-optical and uniaxial stress measurements on 3C SiC : N. The results support a "simplified β-SiC" model for the neutral nitrogen four-particle complex borrowed from work on GaP [111]. Application of uniaxial stress was required to distinguish between an s- and p-like valley–orbit ground state. Evidence for the s-state supports location of the nitrogen impurity on the electron attractive carbon site. Magneto-optical measurements on nitrogen doped 6H SiC using LTPL [112] and absorption [113] support a similar

model in which nitrogen occupies the three inequivalent carbon sites. For luminescence, the initial state is hole-like because the two electrons in the four-particle complex are paired with antiparallel spins. The final neutral donor state exhibits the Zeeman splitting of a single electron. Gorban et al. [114] studied the no-phonon lines of the R and S four particle complexes in 6H SiC by absorption accompanied by application of uniaxial stress. Besides the excited states R_{02} and S_{02} associated with the nearby valence band split off by the small spin−orbit interaction, they argue that two lines R_{03} and S_{03} observed at higher energy are associated with the crystal field split valence band. Application of stress along the three principal directions allowed a determination of the valence band deformation potentials, assuming that the binding energy of the electron to the impurity does not vary with stress. The polarizations of the no-phonon lines R_0, S_0, R_{02}, and S_{02} change with increasing uniaxial stress applied perpendicular to the a-face or prism face from $\mathbf{E} \perp \mathbf{c}$ to $\mathbf{E}$ parallel or perpendicular to the direction of stress. The applied uniaxial stress makes the equivalent electron pockets inequivalent, leading to modifications in the electron wave functions. Haberstroh et al. [115] measured the dependence of the R_0 and S_0 LTPL lines of 6H SiC : N on uniaxial stress. Shifts, but no splittings, were observed.

The pressure dependence of the energy gap varies with polytype. Kobayashi et al. [116] measured the dependence of the indirect absorption edge of n-type 3C SiC on hydrostatic pressure up to 14.3 GPa using a diamond anvil cell. The samples were small pieces of 20 μm thick CVD grown films with the Si substrate removed. The measured first-order pressure coefficient is −1.9 meV/GPa at room temperature, while theoretically calculated values [116 to 119] range from −1.1 to −3.6 meV/GPa. Kobayashi et al. [116] also measured the pressure dependence up to 9.66 GPa of the momentum conserving phonon replicas of the nitrogen four-particle complex by LTPL at 1.8 K. The no-phonon line was not observed, but calculations [120] indicate that the phonon frequencies shift a few meV at 10 GPa. The phonon replica lines follow the shift of the absorption edge up to about 4 GPa, but shift more strongly to lower energies at higher pressures.

Engelbrecht et al. [121] found a linear dependence of the energies of the P_0, R_0, S_0, R_{02}, and S_{02} photoluminescence lines in 6H SiC on hydrostatic pressure up to 5.0 GPa. The samples were grown by the modified Lely method, ground and polished down to 50 μm thickness, and broken into small pieces for insertion into a diamond anvil cell. The measured pressure coefficients at 29 K were 2.0 meV/GPa for P_0, 2.3 meV/GPa for R_0, S_0, and S_{02}, and 2.4 meV/GPa for R_{02}. Since the P_0 complex has the lowest exciton binding energy, they assume that its pressure dependence most closely follows the indirect band gap. Calculated values of the coefficient are 0.8 meV/GPa [121] and −0.3 meV/GPa (at the M point) [119]. Note that the sign of the measured coefficient is positive in 6H SiC, but negative for 3C SiC.

Haynes' rule [122], first applied to silicon, states that there is a relationship, usually linear, between the exciton binding energy to a neutral shallow impurity and the ionization energy. The rule applies to donors and acceptors separately. In GaP, a binary semiconductor, the lines have different slopes and nonzero intercepts [123, 124]. In silicon carbide, Haynes' rule applies for nitrogen donors across polytypes and inequivalent sites. This result seems to call into question proposed explanations [123 to 125] of Haynes' rule based on effective masses and central cell effects.

We now consider fine structure in nitrogen related LTPL spectra. Two-electron transitions (TET), for which the final state after recombination of a four-particle complex is a

neutral nitrogen donor in an excited state, were identified in early work on 3C SiC [56] and studied in detail by Dean et al. [87]. The TETs appear as satellites of the MC phonon replicas. Unlike infrared absorption spectroscopy, both ns and np (n is the principal quantum number) excited states are observed. Analysis of the Zeeman splitting of the $2p_{\pm}$ level provided a measurement of the transverse effective mass. Then a fit using Faulkner's [126] theory led to values for the parallel mass and the static dielectric constant. Dean et al. [127] and Herbert et al. [128] observed sets of satellite lines on both the no-phonon lines and phonon replicas of 3C SiC : N and identified them as signatures of recombination of multiple exciton complexes. Kulakovskii and Gubanov [129, 130] analyzed in detail the dependence of these spectra on temperature and uniaxial stress up to five bound excitons. The principal features were successfully explained by the single particle shell model of Kirczenow [131], but additional splittings introduced by electron–electron and electron–hole exchange were also proposed. Neither TETs nor multiple bound excitons have yet been identified in any other SiC polytype.

The 4N LTPL spectrum is commonly used as a diagnostic indicating the presence of nitrogen, its concentration, as well as crystal or film quality. The spectrum can be calibrated to provide a quantitative measure of nitrogen concentration reliable below the limits of standard techniques such as capacitance–voltage (C–V). Clemen et al. [132] based their calibration for 6H SiC on a linear correlation between the ratio of the intensities of the no-phonon line P_0 to the I_{77} (the subscript indicates the energy of the momentum conserving phonon in meV) replica of the free exciton (the strongest free exciton line) and the net impurity concentration measured by C–V at room temperature. This calibration covered the range 2×10^{14} to $3 \times 10^{16}\,\mathrm{cm}^{-3}$. Extrapolation should be reliable down to $10^{13}\,\mathrm{cm}^{-3}$. Such a calibration is stable over the temperature range 1.3 to 2.14 K, whether based on P_0, Q_0 or S_0. The calibration depends on the equipment and conditions of measurement, and must be redone for each application. Henry et al. [133] based their calibration for 6H SiC : N on the combined areas under R_0 and S_0 because they are stronger than P_0. The areas were estimated by multiplying the peak intensity by the full width at half maximum. The accuracy of this calibration is about 20%. Ivanov et al. [134] extended this work to include thick 4H SiC films grown by hot-wall CVD. In this case peak heights and widths were obtained by fitting the lines. Broadening associated with the instrumental lineshape was included in the forms of the fitting functions. They found that the PL ratio was directly proportional to the doping concentration measured by C–V for uncompensated films, defined by the absence of the spectrum of the Al four-particle neutral bound exciton complex. They also examined carefully the role of temperature dependence and excitation intensity.

The electronic energy level structure of shallow nitrogen donors in SiC polytypes has been investigated using infrared absorption. For 3C SiC the spectrum is now well characterized and understood. Moore et al. [89 to 91] observed transitions from the $1s(A_1)$ ground state to $np_{\pm}$ up to $n = 6$, np_0 up to $n = 4$, and to $4f_{\pm}$ for nitrogen in 3C SiC at 4.2 K. A successful fit to Faulkner's theory [126] is obtained using the effective masses measured by far infrared cyclotron resonance [88], demonstrating consistency with cyclotron resonance as well as TETs measured by LTPL [87]. As the sample is warmed, a series of transitions originating from the 1s(E) level appears. The measured valley–orbit splitting is 8.34 meV, in agreement with earlier measurements of 8.37 meV by electronic Raman scattering [135] and (8.36 ± 0.3) meV by infrared absorption [136]. The measured binding energy for nitrogen obtained by fitting the data to Faulkner's theory

using $m_\perp/m_\parallel = 0.370$ [88] is (54.2 ± 0.2) meV, in agreement with the value (53.6 ± 0.5) meV measured by Dean et al. [87]. Moore et al. [89 to 91] also measured the absorption spectrum of a second, unidentified donor which has very narrow lines and a binding energy of 47.8 meV, very close to the value 47.2 meV obtained using effective mass theory without a central cell correction. Infrared absorption spectra of shallow nitrogen impurities have been measured recently in 6H [137], 4H [138] and 15R [139] SiC. Some of the lines in 6H SiC had been observed previously [140, 141]. The spectra are organized into series associated with 1s(A_1) and 1s(E) initial states to obtain valley–orbit splittings of 12.6 meV for the h site in 6H SiC, 7.6 meV for the h site in 4H SiC, and 7.7 and 14.2 meV for the two h sites in 15R SiC. In 6H SiC, two additional closely spaced series are classified as transitions originating at 1s(A_1) levels, based on temperature dependence, and identified with nitrogen substituting on the two quasicubic sites k_1 and k_2. Series associated with 1s(E) states are not observed for the k sites. Based on the presently accepted locations of the conduction band minima at M for 4H SiC, at U on the M–L line for 6H SiC, and the calculated [86] position X in the rhombohedral Brillouin zone for 15R SiC, the effective mass tensors are allowed to have three distinct elements based on symmetry. Since Faulkner's theory [126] is based on electron pockets that are ellipsoids of revolution, it does not apply to these polytypes. In the absence of a correct model and given the success with 3C SiC, an attempt was made to fit the IR spectra using Faulkner's theory, leading to a determination of effective mass parameters $m_\perp$ and $m_\parallel$, as well as ionization energies, using the 1s(A_1) series for the hexagonal sites. Recent measurements of effective masses in 4H and 6H SiC by optically detected cyclotron resonance [83, 95, 96], a more direct method, called into question the values derived from the IR measurements. However, the nitrogen ionization energies obtained from the fits are not as model sensitive and should be reliable to within a few meV. Evidence of this agreement is the consistency with Hall effect data [137 to 139]. The applicability of effective mass theory to a polytype with a large unit cell was questioned by Patrick [97]. The Bohr radius for an effective mass donor in 3C SiC is about 15 Å. Corrections to effective mass theory tend to reduce the size of the ground state wave function. For 6H SiC the period along the *c*-axis is about 15.1 Å. Thus, the local environment sampled by an electron in a donor ground state will depend on the impurity site, particularly for long period polytypes. This effect will be reduced somewhat for excited states due to their larger size, but may still play a role. Note that the excited state ladders of nitrogen donors in 4H and 6H SiC for the h and k sites differ. Götz et al. [142] observed strong impurity related vibrational modes in 4H SiC. Vibrational transitions are distinguished from electronic transitions by studying the temperature dependence of the spectrum. Engelbrecht and Helbig [143] reported similar results for 6H SiC. Engelbrecht et al. [144] examined the dependence of the infrared absorption spectra of nitrogen-doped 6H SiC on magnetic field up to 20 T. No Zeeman splittings were observed. This result is consistent with an electron effective mass tensor with three distinct diagonal elements, which would break the symmetry responsible for the $p_\pm$ orbital degeneracy in Faulkner's theory. Four of the lines undergo a strong quadratic shift with magnetic field for $\mathbf{B} \parallel \mathbf{c}$. There is no shift for $\mathbf{B} \perp \mathbf{c}$. By analogy with the quadratic Zeeman effect in Si, they conclude that the long axis of the electron pockets, corresponding to the largest effective mass, is oriented along the *c*-axis.

Srichaikul and Chen [85, 145, 146] recently calculated nitrogen donor binding energies in 3C, 4H, 6H and 2H SiC. Wave functions at the conduction band minima were ob-

tained using a hybrid pseudopotential tight binding model [145]. Corrections to effective mass theory include the central cell potential, the pocket wave function and the valley–orbit interaction. The elements of the electron effective mass tensor were parameters in the calculations. Both calculated and measured effective masses were used to calculate the ionization energies for nitrogen donors at each of the inequivalent sites. Reasonable agreement was obtained with experiment when reliable effective masses were used. This calculation represents real progress even in its present early state because it allows the possibility of gaining a physical understanding for the site dependence and effective mass dependence of donor properties across polytypes as well as the possibility of associating measured spectra with specific sites. Such work should be extended to the remaining states of the ground state multiplet (e.g., to the 1s(E) levels for the hexagonal polytypes) to determine theoretically the valley–orbit splittings and to the excited states to interpret the infrared absorption measurements. Such extensions are not easy because conduction bands closely spaced in energy to the minima must be included. For 6H SiC the nonparabolic nature of the conduction band along the k_z direction must be taken into account. Once spectra of neutral shallow impurities are understood, one can hope for extension to neutral four-particle donor and acceptor complexes.

In conclusion, while much is known about nitrogen as a substitutional donor in SiC polytypes, and it is certainly the best understood impurity in SiC, a great deal of important information must be obtained and verified to complete the knowledge base.

6. Phosphorus

Based on measures of size such as the covalent radius, phosphorus is expected to substitute preferentially on the silicon sublattice in SiC. Phosphorus can be introduced into SiC during CVD growth, by ion implantation, diffusion, and neutron transmutation of Si. In the last case added P clearly replaces Si. At present the literature does not give a complete and consistent picture of the location of P in the SiC lattice as an isolated impurity, how it participates in complexes, and the corresponding electronic level structures. ESR and ENDOR have been performed on n-type compensated 6H SiC crystals doped with P by neutron transmutation and subsequently annealed [147 to 150]. Two distinct spectra were observed. One is interpreted as an axially symmetric phosphorus–carbon vacancy complex, observed for both h and k sites. The other spectrum is interpreted as substitutional phosphorus on the Si k site (by analogy with nitrogen) with a binding energy of about 100 meV, somewhat less than the value for nitrogen. Sonntag and Kalbitzer [151] measured the temperature dependence of the electrical conductivity in nominally undoped 6H SiC ion implanted with phosphorus at room temperature and obtained an activation energy of about 0.21 eV. Troffer et al. [152] implanted p-type Al-doped 6H SiC epilayers with phosphorus and characterized them after annealing by Hall effect, admittance spectroscopy and LTPL. Analysis of the Hall and admittance data yields two ionization energies, (80 ± 5) meV and (110 ± 5) meV, associated with the hexagonal and two unresolved quasicubic sites, respectively, by analogy with nitrogen. The best fit to the neutrality equation was obtained by setting the concentration of the impurity with the deeper level about twice as great as the shallow impurity. Four lines observed by Troffer et al. [152] with LTPL at 1.9 K over the interval 420 to 421 nm increase with annealing temperature up to 1700 °C. When 1.5 μm is removed from the surface (greater than the depth of the implanted phosphorus), these lines disappear. One

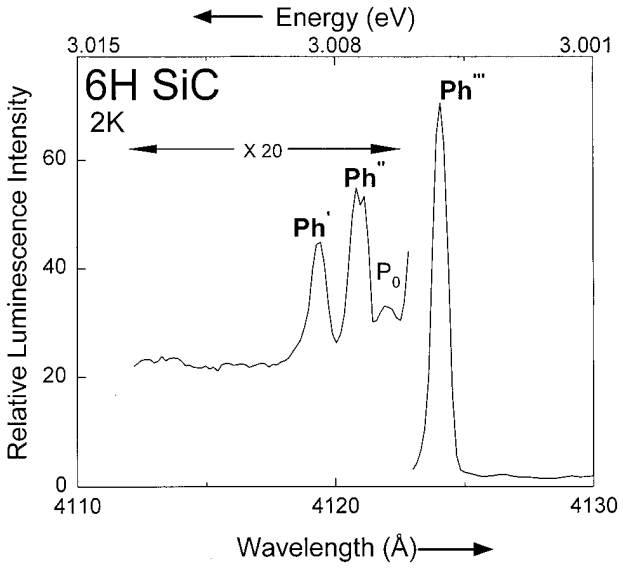

Fig. 3. Low temperature photoluminescence spectrum of a 6H SiC homoepitaxial film grown by chemical vapor deposition with PH_3 added to the flow. The peaks labeled Ph′, Ph″ and Ph‴ are no-phonon lines of the neutral phosphorus four-particle bound exciton complex for phosphorus replacing silicon. P_0 is a no-phonon line of the neutral nitrogen donor four-particle complex (4N). Note that the two lines at the shortest wavelengths, Ph′ and Ph″, are most closely spaced, in contrast to the spacings between P_0, R_0 and S_0 of the 4N complex

must be very cautious when associating spectral lines with the implanted ion. In our laboratory we have observed this spectrum for samples implanted with P, B, He, Li, O and Er.

We report a new phosphorus-related spectrum observed by LTPL on 6H SiC homoepitaxial films doped using PH_3 during CVD growth [153]. Fig. 3 shows a spectrum recorded at 2 K. The line labeled P_0 is a no-phonon line of the neutral nitrogen four-particle complex at the hexagonal site. The three lines labeled Ph′, Ph″, and Ph‴, which increase in intensity with added phosphorus, are no-phonon lines of neutral four-particle complexes for phosphorus substituting on the two k sites and the h site presumably of the Si sublattice. The close spacing of the lines Ph′ and Ph″ suggests that they may be identified with the two quasicubic sites. In contrast with nitrogen, the exciton binding energies to the k-site phosphorus donors is less than for the h site according to this interpretation. Assuming that Haynes' rule applies to Si site donors, the donor ionization energy for phosphorus is smaller for the quasicubic sites, which is opposite to the behavior of carbon site nitrogen donors. Further details regarding the optical signatures of phosphorus in SiC, including phonon replicas, temperature dependence, magneto-optics, and polytype dependence are to be published shortly [153].

7. Shallow Acceptors: Aluminum and Gallium

Although Al and Ga acceptors in SiC are not that shallow we will refer to them as such because some of their properties are effective mass like.

The level structure of shallow acceptors is determined in part by the valence band structure near the maximum. The valence band maximum for all of the important silicon carbide polytypes is located at (or very near) the point Γ at the center of the Brillouin zone. At the level of band structure calculations with accuracy of a few tenths of an eV, the top of the valence band is a degenerate triplet of p-like states. The uniaxial structure of the hexagonal and rhombohedral polytypes leads to a crystal field splitting

into an orbital doublet ($P_{\pm}$) and a singlet (P_0) at lower energy. The crystal field splitting is expected to increase with hexagonality. When electron spin is included, we have a sixfold set of states with spin–orbit coupling. The spin–orbit splitting is small in SiC polytypes, 10 meV for 3C SiC and 7 meV for 6H and 15R SiC [68, 69], indicating that the electron density associated with the highest valence bands is largely located on the carbon sublattice [54]. For 3C SiC, the resulting valence band structure including spin is a fourfold degenerate band at the point $\mathbf{\Gamma}$ in the Brillouin zone (heavy and light holes) typical of zincblende semiconductors with a twofold degenerate spin–orbit split-off band below. The symmetry labels in the group T_d [154] are $\mathbf{\Gamma}_8\,(j = 3/2)$ and $\mathbf{\Gamma}_7\,(j = 1/2)$, respectively. For the hexagonal and rhombohedral polytypes, there are three closely spaced doubly degenerate valence bands at $\mathbf{\Gamma}$, similar to CdS [155], labeled A, B, and C in order of decreasing energy or, equivalently, $\mathbf{\Gamma}_9$, $\mathbf{\Gamma}_7$ and $\mathbf{\Gamma}_7$ for the point group C_{6v}. The crystal field splittings in SiC have not been measured reliably and accurately. Theoretical calculations of the valence band structure near the maximum at this level of detail have been performed only recently [32, 64, 64a]. Here we have described the valence band structure according to Hopfield's quasicubic model [156] for a uniaxial semiconductor. The method of invariants [157] may be used to construct model Hamiltonians including finer levels of detail, **k**-space dependence, and external perturbations, with parameters to be determined from band structure calculations or experiment.

The valence band structure has not been examined by hole cyclotron resonance in any SiC polytype. The energy levels of shallow acceptors have been measured and calculated for many semiconductors [158], but such work has not yet been possible in SiC. However, four-particle neutral acceptor bound exciton complexes have now been observed in several polytypes for both Al and Ga. The four particles are the negatively charged acceptor ion, its hole, and the electron–hole pair of the attached exciton. The two holes are identical so that the exciton loses its distinct identity when its energy becomes localized at a neutral acceptor. The systematic observation of the neutral aluminum four-particle complex 4Al became possible once the CVD growth of lightly p-doped SiC films with low nitrogen background was achieved. Clemen et al. [159 to 161] observed the 4Al complex in 3C, 4H, 6H, and 15R SiC. In 3C SiC at least five closely spaced no-phonon lines are observed at high resolution using ultrahigh vacuum low temperature cathodoluminescence [160]. At least 15 sharp no-phonon lines of 4 Al are observed [159 to 161] in the LTPL spectrum of 6H SiC between the P_0 and R_0, S_0 lines of nitrogen. Although these spectra presumably include Al substituting for Si at all three inequivalent sites, the lines have not been convincingly sorted out with respect to site. At least 22 4Al no-phonon lines are observed in 15R SiC [161], but only a few no-phonon lines have been resolved in 4H SiC [160, 161]. The no-phonon, 4Al lines for the noncubic polytypes are preferentially polarized with $\mathbf{E} \perp \mathbf{c}$, most strongly so for 6H SiC. Although isolated substitutional Al introduces a much deeper level than does nitrogen, the quite comparable binding energies of excitons to N and Al are consistent with Haynes' rule if one considers the proper analogy with GaP [123, 162] rather than the more well-known case of Si [122]. The 4Al no-phonon spectrum was also observed quite early on by Haberstroh et al. [115] in 6H, 4H, and 15R SiC. It was first reported in 6H SiC Lely samples by Bogdanov and Gubanov [163], but misidentified as multiple bound exciton satellite lines of P_0. Multiple bound exciton lines are weaker than the corresponding principal bound exciton line. The 4Al spectrum is prominent only in p-type material and can be stronger than P_0, eliminating the mechanism of multiple bound excitons.

The multiplicity of 4Al no-phonon lines is qualitatively explained by a model originally applied to neutral acceptor bound exciton complexes in GaP by Dean et al. [123]. Their analysis based on symmetry considerations and the couplings between the particles making up the complex can be carried over without change to 3C SiC, but must be reformulated for application to the noncubic polytypes [159]. An assignment of lines to specific transitions was not possible in GaP, and is more difficult in SiC due to the inequivalent sites in all noncubic polytypes except for 2H SiC.

Phonon replicas of 4Al have been observed [160], consistent with the momentum conserving phonons of the 4N complex and in support of the identification of this spectrum as a neutral four-particle aluminum complex. The no-phonon lines of 4Al are relatively stronger with respect to the phonon replicas compared to 4N.

Zeeman spectroscopy has been performed [159, 164] on samples of lightly doped p-type 6H SiC showing particularly sharp 4Al no phonon lines using magnetic fields up to 6T with orientations $\mathbf{H} \parallel \mathbf{c}$ and $\mathbf{H} \perp \mathbf{c}$. The behavior of the two strongest lines is described by Thomas and Hopfield's [155] picture for neutral acceptor bound exciton recombination originally developed for CdS. In the initial state, the two holes are paired so that the g-factor is associated with the electron, and thus is essentially isotropic. The final state is a neutral acceptor, with the anisotropic g-factor associated with the hole at the top of the Γ_9 valence band. The hole g-factor is zero for $\mathbf{H} \perp \mathbf{c}$. For the two strongest 4Al lines with $\mathbf{H} \perp \mathbf{c}$, g is in fact close to 2, while for $\mathbf{H} \parallel \mathbf{c}$ g is zero to within the resolution of the measurement. This result is consistent with the values for g measured by Dang et al. [165] using ODMR for the Al acceptor in 6H SiC. The magneto-optical behavior of the many other lines making up the 4Al no-phonon spectrum has not been analyzed in detail.

Recently the neutral four particle gallium complex 4Ga has been observed in 3C, 4H and 6H SiC using photoluminescence [166, 167]. Thick, high quality epitaxial films with low background doping were grown in a hot-wall CVD reactor with trimethylgallium (TMG) added to the flow. The no-phonon lines appear in the same spectral region as 4Al, but a little deeper, and are polarized predominantly with $\mathbf{E} \perp \mathbf{c}$ in 6H SiC. The binding energies of holes to Ga acceptors in SiC polytypes are also deeper than for Al. Al and Ga fall on the same line on a Haynes' rule plot of exciton binding energy versus hole ionization energy independent of polytype. Weak phonon replicas of 4Ga in 6H SiC were observed at 77, 97 and 106 meV. As the temperature is raised, the intensity of the 4Ga spectrum in 6H SiC begins to decrease at 25 K and is completely quenched above 85 K. An interesting feature of the no-phonon spectrum of 4Ga is that two distinct spectra [167] are observed in different samples of 6H SiC. The spectrum with more lines appears to be related to the simpler spectrum by splitting of some of the lines. Although a similar effect is observed for the 4Al complex [159, 164], the observation of splittings in 4Ga spectra is correlated with high Ga acceptor concentration. Henry et al. [167] propose that the splittings are associated with Ga substituting at the two quasicubic sites in 6H SiC. Work on magneto-optics of the 4Ga complex is in progress.

Analysis of the temperature dependence of free to bound transitions from the conduction band to a neutral acceptor can provide a value for the acceptor ionization energy accurate to about 1 meV. For SiC, overlapping of closely spaced peaks due to inequivalent sites can introduce additional uncertainty. In the standard model [105, 168 to 170], the energy dependence of the luminescence intensity is

$$I(E) = N_{\mathrm{A}} n(E)\, \sigma(E)\, \nu_{\mathrm{th}}(E)\,,$$

where N_A is the concentration of neutral acceptors, $n(E)$ the density of conduction electrons per unit energy, $\sigma(E)$ the cross section for radiative capture of a conduction electron by the neutral acceptor, and $\nu_{th}(E)$ the thermal speed of a conduction electron. The energy E is measured relative to the bottom of the conduction band. For parabolic conduction bands and nondegenerate statistics $n(E) \propto \sqrt{E} \exp(-E/kT)$ and $\nu_{th} \propto \sqrt{E}$. If $\sigma(E) \propto E^m$, then

$$I(E) \propto E^{m+1} \exp(-E/kT),$$

which takes on its maximum value at $E = (m+1)\,kT$. Thus, the peak for free to bound transitions is at energy

$$E_p = E_{GX} + E_X - E_A + (m+1)\,kT,$$

where E_{GX} is the exciton energy gap, E_X the free exciton binding energy, and E_A the acceptor binding energy. Typically the value $m = -1/2$ is used. In applying this equation to extrapolate back to $T = 0$, one must also take into account the temperature dependence of the exciton gap. At present the dominant uncertainty in measurements of acceptor binding energies in SiC by this method is the lack of a reliable, accurate value of E_X for most polytypes. In early work, Ikeda et al. [105, 170] determined binding energies for Al and Ga in 3C, 6H, 4H, and 15R SiC by this method and provide extensive references to previous work. By fitting the luminescence spectra and also making use of broad distant donor–acceptor pairs peaks, they claim some success in resolving the contributions of the inequivalent sites. Recently, Clemen et al. [161, 164] determined the binding energies of the Al acceptor in 3C and 4H SiC epitaxial films as $E_A(3C) = (269 \pm 2)$ meV and $E_A(4H) - E_X = (176 \pm 2)$ meV, where E_X is the binding energy of the free exciton. In agreement with Ikeda et al. [105], only a single broad peak was observed in 4H SiC. Yoganathan et al. [171] found that N, Al, and B free to bound luminescence dominates the room temperature electroluminescence spectra of moderately nitrogen-doped (1×10^{17} cm^{-3}) 3C and 6H SiC p^+–n diodes. The contributions of these impurities to the electroluminescence vary with forward current, as the location within the device of the dominant radiative recombination changes.

Donor–acceptor pair (DAP) spectra contain a great deal of information about impurities. Dean [172] has written a comprehensive review. The analysis of close pair spectra was first applied to GaP by Hopfield et al. [173]. The energy of the emitted photon is

$$h\nu = E_G - (E_D + E_A) - E_C + E_{vdW},$$

where E_C is the Coulomb interaction energy between the ionized donor and acceptor after recombination and E_{vdW} is the van der Waals interaction energy between the neutral donor and acceptor before recombination. For moderately separated pairs, $E_C = -e^2/\varepsilon r$, where ε is the static dielectric constant and r is the pair separation. For substitutional impurities there is a shell structure of spacings leading to a multitude of spectral lines. The zincblende and wurtzite shell structure spacings have been given by Henry et al. [174] and Wiley and Seman [175]. For SiC, a binary semiconductor, impurities may substitute on either the Si or C sublattices. If both the donor and acceptor substitute on the same sublattice, the spectrum is called Type I. For substitution on opposite sublattices the spectrum is Type II. For all polytypes but 3C and 2H SiC, there are inequivalent sites on each sublattice, leading to additional complexity and difficulty of analysis. For the closest pairs, Patrick [176] introduced multipole corrections to the

Coulomb potential to account for splittings within shells. The van der Waals term is usually taken as proportional to r^{-6}, without further corrections. After assigning the resolved shells, the photon energies can be fitted to the above equation and extrapolated to pairs with infinite separation to obtain

$$h\nu_\infty = E_G - (E_D + E_A)\,.$$

The accuracy of the determination of the sum of the donor and acceptor binding energies is limited by the uncertainty of the free exciton binding energy E_X, since the exciton gap $E_{GX} = E_G - E_X$ is known precisely for the important SiC polytypes.

For 3C SiC the N–Al close pairs DAP spectrum measured at 1.8 K has been analyzed in detail [177]. It is Type II. Since nitrogen is known to substitute on the carbon sublattice, Al replaces Si. The limiting photon energy is $h\nu_\infty = 2.0934$ eV. The exciton energy gap at $T = 1.8$ K is 2.390 eV. Since $E_D = 54$ meV for nitrogen [87, 89, 90] and $E_X = 27$ meV for the free exciton [69], $E_A = 270$ meV for Al in 3C SiC. Details and anomalies in the intensities of the shell structure lines may provide information about the wave functions of donors and acceptors, if they could be analyzed. Kuwabara et al. [178] measured and analyzed the N–Ga DAP spectrum in 3C SiC. It is Type II, so Ga replaces Si. From the sharp line spectrum, they determined $h\nu_\infty = 2.0038$ eV, so that $E_A(\mathrm{Ga}) = 359$ meV, using the values for E_{GX}, E_X, and $E_D(\mathrm{N})$ given earlier. Fig. 4 and 5 show examples of excellent N–Al DAP spectra, measured in our laboratory, of single crystal 4H and 6H epitaxial films. It has not been possible to analyze these spectra, in part due to inequivalent sites. For example, since there are three inequivalent sublattice sites in 6H SiC, there should be nine distinct overlapping DAP spectra. Observation and successful analysis of DAP spectra in 2H SiC may be a necessary first step before progress is possible for the other noncubic polytypes.

Most of the intensity for DAP recombination appears in the no-phonon distant pairs peak and its phonon replicas. DAP peaks may be roughly but not definitely identified by their characteristic dependence on the excitation intensity. With increasing intensity, the emission of the most distant pairs saturates first due to their relatively long decay

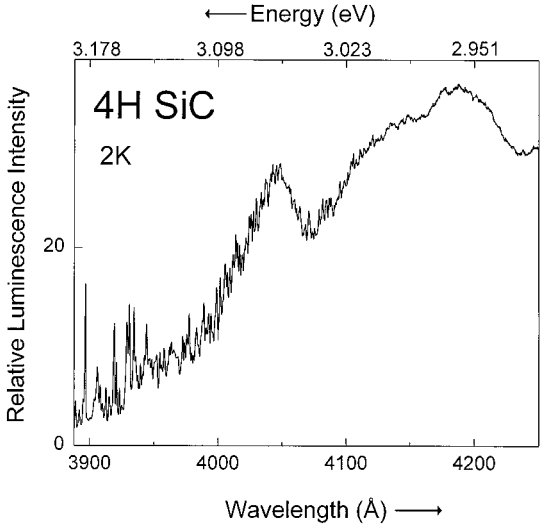

Fig. 4. Low temperature photoluminescence spectrum of a p-type 4H SiC CVD grown homoepitaxial film showing both sharp peaks due to the shell structure of closely spaced donor–acceptor pairs and broad peaks due to distant pairs and their phonon replicas. It should be noted that the noise level is very low and all sharp lines are due to donor–acceptor pairs and *not* noise. The fact that we see sharp structure superimposed on the broad peak at 4050 Å is likely due to the overlapping of DAPs from various inequivalent sites

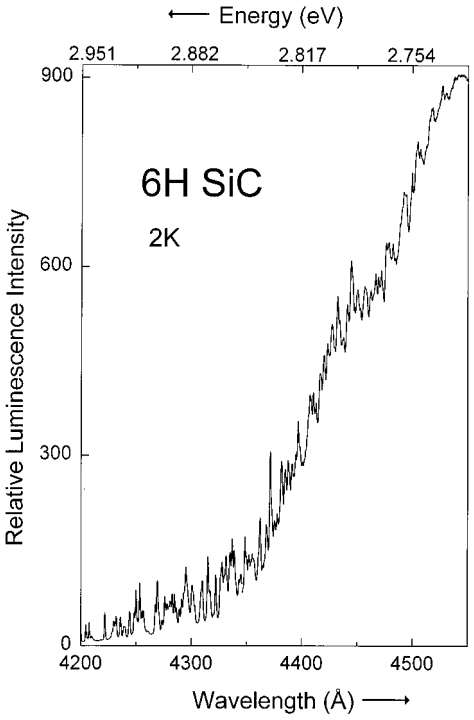

Fig. 5. Low temperature photoluminescence spectrum of a p-type 6H SiC CVD homoepitaxial film showing sharp peaks due to the shell structure of donor–acceptor pairs. As in Fig. 4, the overlapping of sharp structure on the broad peak at 4450 Å indicates the participation of various inequivalent sites

times, leading to a blue shift and broadening of the peak as the energy is pushed into the closer pairs. For distant pairs, the recombination rate decreases exponentially with separation due to the exponentially decreasing wave function overlap between the donor and acceptor. When the excitation source is abruptly turned off, the decay of the DAP peak exhibits a nonexponential tail at long times, and the spectrum redshifts as the decay proceeds. With increasing temperature, a DAP peak disappears as the shallower of the two impurities ionizes. The corresponding free to bound peak grows. Zanmarchi [179] clarified the relationship between the N–Al DAP and Al free to bound spectra in 3C SiC. Ikeda et al. [105, 170] analyzed DAP peaks in Al and Ga-doped 3C, 4H, 6H, and 15R SiC. Having first estimated acceptor ionization energies from the free to bound peaks, they performed curve fits to estimate the nitrogen donor binding energies. For 4H, 6H, and 15R SiC, they assumed that the two principal no-phonon peaks, which they called B_0 and C_0, are associated with nitrogen substituting at hexagonal and quasicubic sites, respectively. Just as for the free to bound transitions, fine structure in these broad no-phonon peaks, when observed, was identified with acceptors occupying inequivalent sites. Two N donor binding energies were obtained from their fits to B_0 and C_0. The claimed accuracy of ± 3 meV for these values is questionable due to the lack of reliable values for the free exciton binding energies and the width and overlap of the peaks under consideration.

Insight into the nature of Al acceptor states in bulk 6H SiC was obtained by performing optical detection of magnetic resonance (ODMR) using the 2.65 eV N–Al DAP band. In addition to the isotropic nitrogen donor resonance ($g = 2.004 \pm 0.002$), Dang et al. [165] observed three anisotropic resonances ($g_{\|} = 2.412 \pm 0.002$, 2.400 ± 0.002, and 2.325 ± 0.002; $g_{\perp} = 0$) associated with Al substituting at the three inequivalent silicon sites. The anisotropy reflects that of the free hole state from the top of the highest valence band and is thus evidence of the effective mass character of the Al acceptor. The reduction of $g_{\|}$ from the value 4.0 for the free hole is associated with quenching of the orbital angular momentum through binding of the hole, possibly by the dynamic Jahn-Teller effect as proposed by Morgan [180]. About the same time, Scott et al. [181] ob-

served electronic transitions with zero field values 1.12, 1.32, and 1.50 meV and $g = 1.97$ (isotropic) in Al-doped 6H SiC using magneto-Raman scattering and suggested that they are spin-flip transitions in excitons bound to isoelectronic Ti traps at the three inequivalent Si sites. Dang et al. [165] and Scott et al. [182] reinterpreted the lines as orbital transitions of holes at Al acceptors. The zero field splittings indicate that the spin−orbit splitting is strongly quenched by the same mechanism acting on the bound holes in ODMR [165]. A simple model provides consistency between the ODMR and magneto-Raman data, lending support to this interpretation. Recently, Reinke et al. [183] studied Al-doped 6H and 4H SiC by ODMR, magnetic circular dichroic absorption (MCDA) and MCDA-EPR. They observed three sets of lines with hyperfine splittings in 6H SiC and two in 4H by MCDA-EPR, and interpreted them as Al with nuclear spin $I = 1/2$ associated with inequivalent sites. Analysis of the hyperfine splittings indicates that the electron density is low at the Al, indicative of an effective mass like state. The slightly larger values of $g_{\|}$ measured for 4H SiC correlate with the shallower binding energy with respect to 6H SiC obtained by Ikeda et al. [105]. The ODMR results agreed with Dang et al. [165] for 6H SiC; no ODMR spectrum was observed in 4H SiC. Baranov et al. [184] observed ODMR as well as hyperfine splitting using a derivative technique for Ga-doped 6H SiC. The results suggest that Ga is an effective mass like acceptor. There are only two ODMR spectra, not three. The values of $g_{\|}$, 2.27 and 2.21, are smaller than for Al, and $g_{\perp} = 0.6 \pm 0.2$, not zero, for both. Thus, the story for Ga is not as clear as for Al at this time.

8. Boron

Although boron has been used as a p-type dopant since the 1950s, much has been learned about the nature of B in SiC only recently. It was clear since the 1960s that B introduces at least two levels in SiC, one relatively shallow, the other deep. Lomakina [185] measured an ionization energy of 390 meV for B-doped 6H SiC using the temperature dependent Hall effect. On the other hand, B-doped 6H SiC LEDs fabricated at General Electric in Cleveland [186] emitted in the yellow, with a peak near 5900 Å. Interpretation of this emission as free conduction electron to neutral boron transitions leads to an ionization energy for B of about 700 meV. Yamada and Kuwabara [187] measured and analyzed the N−B DAP spectrum in 3C SiC. It is a Type I spectrum, implying that for the deep boron level B substitutes on the carbon sublattice. Using the known values for the band gap and nitrogen donor binding energy, the acceptor ionization energy $E_{\mathrm{A}}(\mathrm{B}) = 749$ meV is obtained for B in 3C SiC. Kuwabara and Yamada [188] also measured and analyzed the temperature dependence of the free to bound peak to obtain the value $E_{\mathrm{A}}(\mathrm{B}) = 748$ meV. Ikeda et al. [105, 170] measured and analyzed peaks associated with N−B distant pairs and free electron to neutral B transitions in B-doped 3C, 6H, 4H, and 15R SiC and obtained values for the deep boron ionization energies. They used curve fitting to extract values from broad, overlapping features and attempted to associate the ionization energies with inequivalent sites. While the details of interpretation and precision of values may be questioned, the observation of DAP and FB transitions in four polytypes associated with deep boron is an important result.

It is now clear that B may replace either C or Si in SiC. B-induced centers may not be simple substitutional impurities. The covalent radii of B, C and Si are 0.82, 0.77 and 1.11 Å, respectively. Thus, it is quite reasonable to expect significant, possibly symmetry reducing distortions in the local environment and perhaps an off-center location when B

replaces Si. The deep center is associated with B_C, the shallow level with B_{Si}. Where the B goes depends on the growth conditions. Carbon-rich growth conditions favor B replacing Si, and vice versa. Missing until recently is an optical signature for shallow B.

Sridhara et al. [189] have observed luminescence spectra at low temperatures associated with shallow boron in 4H SiC. 4H SiC homo-epitaxial films were intentionally doped preferentially with either shallow or deep boron by controlling the silicon to carbon source gas ratio during chemical vapor deposition, based on site competition epitaxy. The combination of temperature dependent Hall effect, admittance spectroscopy and deep level transcient spectroscopy indicates that most of the detected boron is in the shallow state for samples grown at a low Si/C ratio. For these samples a peak appears near 3838 Å in the LTPL spectrum. Fig. 6 shows a spectrum with a sharp shallow B peak. Further experiments support the identification of this line with the no-phonon recombination of a neutral boron four-particle (bound exciton) complex: 1. The intensity of the feature at 3838 Å grows with added boron. 2. Momentum conserving phonon replicas are observed, suggesting that the electron is weakly bound. 3. When the temperature is increased excited states are observed, just as for the neutral Al and Ga four-particle complexes. However, the point associated with this shallow boron center on a plot of exciton binding energy versus acceptor ionization energy does not fall on the Haynes' rule linear relationship obeyed by Al and Ga. The shallow boron spectrum is sensitive to the local environments of the B impurities and to temperature. Most often the no-phonon line in 4H SiC appears as a broad peak near 3838 Å, rather than the sharp feature shown in Fig. 6, which is observed only occasionally. Although the shallow boron level is deeper than Al, the shallow boron spectrum is greatly attenuated by $T = 37$ K, whereas the $4Al_0$ spectrum, while broadened, is still strong at $T = 95$ K. This behavior hints at an unusual, easily disturbed structure for shallow boron. Much work

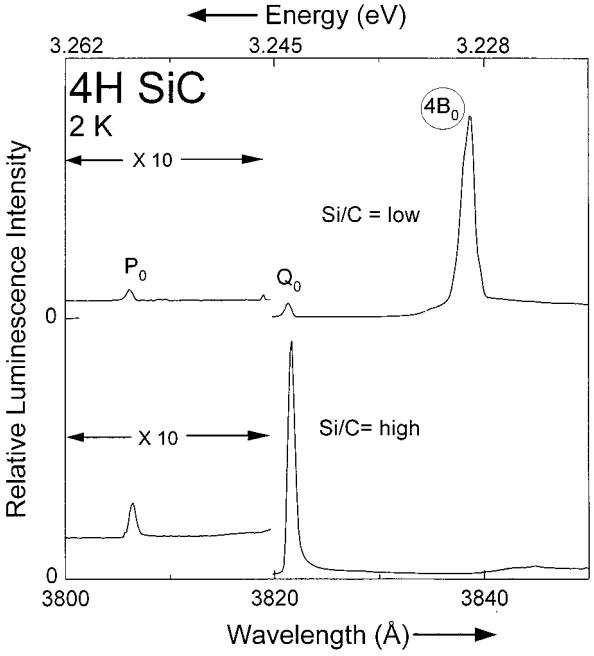

Fig. 6. Low temperature photoluminescence spectra of two boron-doped 4H SiC homoepitaxial films, grown by CVD using two very different Si/C source gas ratios. The peaks labeled P_0 and Q_0 are no-phonon lines of the neutral nitrogen donor four-particle bound exciton complex (4N). The sharp peak at 3838 Å labeled $4B_0$ is associated with no-phonon recombination of the neutral shallow boron acceptor four-particle bound exciton complex, with boron replacing silicon. The dependence of the relative strengths of the $4N_0$ and $4B_0$ lines on the Si/C ratio agrees with the site competition epitaxy growth model for a carbon site donor and a silicon site acceptor. The baseline of the "Si/C = low" spectrum has been shifted for clarity

on electron spin resonance performed on B replacing Si, reviewed elsewhere in this volume, points towards a similar conclusion.

We have also observed a broad feature with an extended tail on the long wavelength side in the LTPL spectrum associated with shallow boron in 15R and 6H SiC. For reasons not understood, the intensities of these features are weak compared to the 3838 Å line in 4H SiC for epi-films grown at the same time. For 6H SiC this boron peak is superimposed on the R_0 and S_0 lines of the 4N complex, which certainly delayed its discovery.

For 4H SiC homoepitaxial films grown with a high Si/C ratio, which favors B_C, the B–N DAP luminescence spectrum is observed at low temperature. It has not been possible to analyze the multitude of sharp peaks associated with close pairs. The intensity of the distant pairs peak decreases with increasing temperature, while a new peak at 2.64 eV, associated with deep boron free to bound transitions, becomes prominent. Analysis of the temperature dependence of the peak position, taking into account the temperature dependence of the exciton gap, leads to the value $E_A(B) - E_X = (628 \pm 1)$ meV, in agreement with the value obtained by Ikeda et al. [105]. Separate peaks for the hexagonal and quasicubic sites are not resolved. The free exciton binding energy E_X for 4H SiC is not known reliably.

Larkin et al. [190] demonstrated that the incorporation of boron into 6H SiC during CVD homoepitaxial growth onto the (0001) Si surface of a boule derived wafer depends on the Si/C ratio. Since the concentration of boron, measured by SIMS or inferred by the concentration of free holes p measured by C–V, is inversely proportional to the Si/C ratio, boron shows a strong preference for replacing Si under these growth conditions, based on the mechanism of site competition epitaxy [98]. LTPL spectra for these films show strong hydrogen lines. The intensity of the strongest hydrogen line, H_3 at 4193 Å [191 to 193], increases with the concentration of diborane used during growth at a fixed Si/C ratio. After a high temperature anneal at 1700 °C, SIMS data show that the hydrogen has left the film, but diffusion of the boron is minimal. LTPL spectra show that a small amount of hydrogen remains in the films. According to C–V data, $N_A - N_D$ increased by a factor of three to four after annealing, indicating that hydrogen passivates the shallow boron acceptor. A tail observed on the low energy side of the 4N LTPL peak S_0 is now believed to indicate the presence of the shallow boron acceptor.

9. Erbium

Among the rare earths, erbium attracts the greatest attention [194, 195] as a semiconductor dopant due to its intra-4f shell emission band near 1.54 μm, coinciding with the loss minimum of silica fibers. In SiC erbium takes on the valence Er^{3+}. No change of valence charge state with the position of the Fermi level, varied by n- and p-type doping, has been observed. Because the $4f^{11}$ electrons are effectively screened from their environment, the description of the electronic structure of an Er^{3+} ion in the crystal can begin with the free ion [196, 197]. The effects of the crystalline environment are added as a perturbation. The level structure is calculated in the intermediate coupling regime, for which the Coulomb and spin–orbit interactions of the 4f electrons are of comparable magnitude. The Russell-Saunders notation is used to label the multiplets of states, but the energy eigenfunctions include contributions from other Russell-Saunders terms having the same J. This mixing is especially strong if the terms are closely spaced in energy.

The ground state multiplet of Er^{3+} is $^4I_{15/2}$, in agreement with Hund's rules. If it is possible to measure a good number of these multiplets in absorption, the Judd-Ofelt theory [198, 199] may be used to fit the spectrum and provide parameters for a free ion Hamiltonian which may be used to calculate the emission spectrum. In a crystalline environment, the degeneracies of the terms are reduced by crystal field splittings. Lea et al. [200] calculated these splittings for cubic symmetry. Although it is difficult to calculate crystal field splittings from scratch, it is possible to fit a spectrum to the diagrams of Lea et al. and thus obtain parameters of a model Hamiltonian for the multiplet in the crystal field.

Erbium is introduced into SiC by ion implantation [201, 202]. Room temperature implants were performed at the University of Erlangen-Nürnberg using four energies ranging from 1 MeV to 40 keV at fluences of $1 \times 10^{13}\,cm^{-2}$ to appropriate a square profile with a maximum penetration of about 0.3 μm. The samples were epitaxial films of 4H, 6H and 15R SiC and platelets of 3C SiC. Following implantation, the samples were placed in a closed CVD SiC crucible and annealed in pure Ar at 1700 °C for half an hour to obtain the brightest Er^{3+} spectra. Photoluminescence was excited using the 3250 Å line of a He–Cd laser or the 2440 Å line of a frequency doubled argon ion laser, analyzed with a grating monochromator or FTIR spectrometer, and detected by a liquid nitrogen cooled Northcoast Ge detector.

At 2 K sharp line spectra are observed [201 to 203] near 1.54 μm for all four polytypes, associated with transitions from the lowest level of the $^4I_{13/2}$ multiplet to the crystal field split levels of the $^4I_{15/2}$ ground state multiplet. The spectra for 4H, 6H and 15R resemble one another, whereas the Er^{3+} spectrum for the 3C SiC host is quite different. High resolution spectra show additional resolved lines with widths as narrow as 110 μeV. There are too many lines for them all to be associated with an isolated erbium ion in a specific environment, no matter where it is located in the crystal. In 6H SiC, some lines show satellites separated by 13 meV, which are interpreted as electronic transitions accompanied by excitation of a local vibrational mode of the erbium center [202, 203]. As the temperature is raised from 2 K, many additional lines appear, some at higher energies [201, 202]. The new lines are due to transitions originating from higher levels of the $^4I_{13/2}$ multiplet. It is likely that all allowed transitions emit observable intensity at 77 K. Er^{3+} photoluminescence in SiC is observed at 525 K. From a practical point of view, the most significant result is that the integrated intensity from 1.49 to 1.64 μm is essentially temperature independent up to 300 K in 3C, 4H, and 15R SiC and to 400 K for 6H SiC. Thus, optoelectronic devices based on Er^{3+} in SiC promise excellent stability with respect to temperature fluctuations. The temperature dependence of the 1.54 μm spectrum and the integrated intensity have been measured, but we have not yet developed a detailed model. In contrast with Si and other semiconductors [195], implantation of oxygen does not enhance the 1.54 μm Er^{3+} luminescence. There is a correlation [203] between the nitrogen donor concentration up to about $10^{17}\,cm^{-3}$ and the integrated intensity, suggesting the participation of nitrogen donors in the excitation of intra-4f shell Er^{3+} luminescence. The mechanism of energy transfer is not understood.

Intra-4f transitions from higher multiplets of the Er^{3+} ladder to the $^4I_{15/2}$ ground state multiplet are observed in 6H and 4H SiC at 2 and 295 K [203, 204]. Although the band gap exceeds the intra-4f transition energy to the ground state for initial states up to $^2H_{9/2}$ and $^2G_{11/2}$ for 6H and 4H SiC, respectively, the highest observed Er^{3+} transition in both cases is $^2H_{11/2} \rightarrow {}^4I_{15/2}$, near 2.36 eV. The complete list of observed transitions

to the ground state multiplet at 295 K, in order of decreasing energy, is $^2H_{11/2} \rightarrow {}^4I_{15/2}$, $^4S_{3/2} \rightarrow {}^4I_{15/2}$, $^4F_{9/2} \rightarrow {}^4I_{15/2}$, $^4I_{9/2} \rightarrow {}^4I_{15/2}$, $^4I_{11/2} \rightarrow {}^4I_{15/2}$, and $^4I_{13/2} \rightarrow {}^4I_{15/2}$, which includes all multiplets below 2.36 eV. A qualitative model for this result begins with the capture of a conduction electron by a nitrogen donor. The electron is transferred to an erbium-related defect level where it recombines nonradiatively with a hole. The energy of recombination excites the Er^{3+} 4f electrons into the $^2H_{11/2}$ multiplet. Some of this energy goes into radiative transitions to the ground state. In parallel there are decays to lower multiplets on the energy ladder (and possible upconversions) leading to the observation of emission bands from all excited multiplets below $^2H_{11/2}$. The excited state bands provide further information about crystal field splittings. For example, six spectral lines belonging to $^4S_{13/2} \rightarrow {}^4I_{15/2}$ have identical energy separations to a set of lines in $^4I_{13/2} \rightarrow {}^4I_{15/2}$, implying that the two spectra, observed at 2 K in 4H SiC, belong to the same Er^{3+} center.

Room temperature Er^{3+} electroluminescence (EL) is observed in forward biased erbium-implanted 6H SiC p–n junctions [202, 205]. As described earlier, erbium is implanted into n-type epilayers grown on n^+ substrates, which are subsequently annealed in pure Ar at 1700 °C. A p-type layer is deposited on top to form the p–n junction, contacts are made by a proprietary process, and the diode is packaged. The 1.54 μm spectra measured at room temperature on the n/n^+ and $p/n/n^+$ structures by photoluminescence are essentially identical to the EL spectrum. EL is observed at a forward current of 20 μA, and grows with increasing current up to 20 mA, the largest used. The EL tends to saturate with increasing current, particularly above 5 mA. Just as for photoluminescence, the EL increases with nitrogen donor concentration over the range 10^{15} to mid-10^{17} cm^{-3}. The external quantum efficiency was estimated by comparison with a calibrated InGaAsP IRED. The value is 7.5×10^{-6} at 10 μA, comparable to the value reported for GaAs:Er^{3+} [206]. The external quantum efficiency decreases with increasing forward current due to saturation of the EL. The external quantum efficiency might be improved by increasing the volume of the Er-doped region in the device. Intra-4f transitions from excited state

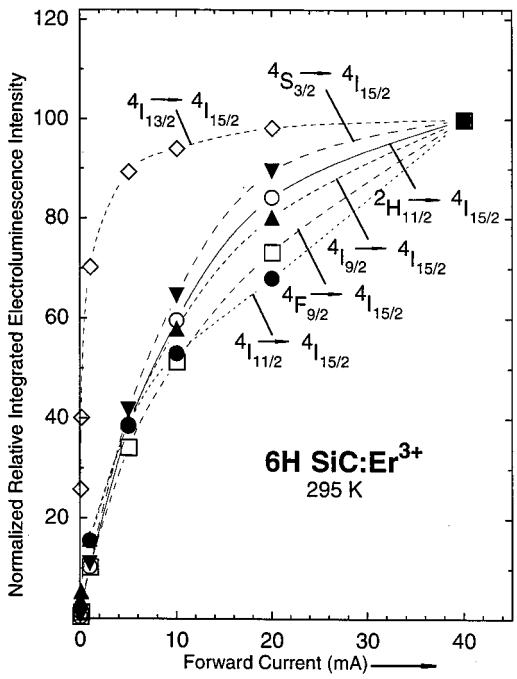

Fig. 7. Forward current dependence of the room temperature relative electroluminescence intensity, integrated over 1.49 to 1.64 μm, of transitions from excited level multiplets to the ground level multiplet in a $p/n/n^+$ 6H SiC:Er^{3+} diode. The transitions are labeled using the conventional Russell-Saunders notation. Data points are indicated using symbols. The lines are guides to the eye

multiplets up to $^2H_{11/2}$ are observed [207]. Fig. 7 shows that the dependence of the integrated EL intensity on forward current is different for each multiplet. The kinetics of energy relaxation have not been analyzed in detail. No 1.54 μm EL is observed under reverse bias breakdown conditions.

Steckl et al. [208] studied the dependence of 1.54 μm Er^{3+} PL on annealing temperature. Erbium was implanted into n-type 6H SiC substrates at the relatively low energy of 330 keV and a fluence of 1×10^{13} cm^{-2}. The depth of the implanted region is about 1000 Å. Samples were annealed in ultrapure Ar for 30 or 60 min at temperatures ranging from 1200 to 1900 °C. The integrated 1.54 μm luminescence intensity drops slightly as the annealing temperature is increased from 1400 °C, perhaps due to outdiffusion of the shallow implanted erbium in these samples. Below 1400 °C the luminescence intensity drops rapidly, although it is still detectable for a sample annealed at 1200 °C. The erbium concentration depth profile was measured by SIMS and analyzed to obtain an estimate of 0.98 eV for the activation energy of Er diffusion in 6H SiC.

It is clear that the study of rare earth impurities in SiC is just beginning. We have recorded a great deal of information in our Er^{3+} emission spectra, but there is little quantitative understanding. An important objective both towards achieving an understanding of the physics of Er^{3+} luminescence in SiC and the development of applications is the successful incorporation of erbium into SiC during growth. The layers obtained by ion implantation are too thin for optimal device performance and the menagerie of luminescent damage-related erbium centers too complex for classification and quantitative analysis.

10. Porous Silicon Carbide

Porous semiconductors have attracted much interest in recent years due to potential applications in optoelectronics and interesting scientific issues. Due to the loss of translational symmetry in a porous material there is a relaxation of selection rules requiring phonon cooperation for optical transitions across an indirect band gap, leading to increased emission or absorption. In addition, particularly for a very fine microstructure (size scale less than 10 nm), there is the possibility of blue shifts due to quantum confinement. Porous silicon, for example, emits quite strongly in the visible. However, the mechanism of luminescence of porous semiconductors is not a settled issue. Contaminating oxides or other deposits on the surface of the finely divided microstructure may well be responsible.

Both n-type [209 to 220] and p-type [216, 221, 222] porous SiC layers have been fabricated, mostly on 6H SiC substrates, although 3C SiC [210, 216] and 4H SiC [216] have also been used. The methods of anodic etching are similar to those used to make porous Si. Typical layer thicknesses range from 1 to 10 μm. For example, Shor et al. [209] etched n-6H SiC (nitrogen doped to 3×10^{18} cm^{-3}) in 2.5% HF in water in the presence of uv light and used transmission electron microscopy to observe feature sizes of 10 to 30 nm. The ultraviolet light produces the supply of holes required at the surface for the reaction to proceed [215]. Shor et al. [221, 222] also prepared porous p-type 6H SiC by anodization in dilute HF using current densities ranging from 5 to 150 mA/cm^2, without uv illumination. Konstantinov et al. [215, 217] discuss the mechanism of etching leading to the formation of micropores.

Light emission by porous SiC has been observed by photoluminescence (PL) [210 to 214, 216 to 219], electroluminescence (EL) [214, 218], and cathodoluminescence [209,

221, 222]. The results have been disappointing with respect to ultraviolet emission beyond the bulk band gap due to quantum confinement of carriers. Generally, a broad peak is observed in the blue–green for porous 6H SiC. In some cases the emission is quite strong compared to the emission of the bulk crystal; in others the emission is weak. Electroluminescence is typically produced using an electrolyte–SiC junction. Although there is relatively stronger emission at higher frequencies for the porous layers with the smallest microstructural features [216, 217], there is little or no emission beyond the bulk band gap. Konstantinov et al. [216, 217] found that the PL spectra for 3C, 6H, and 4H SiC are similar even though the band gap energies differ by up to 0.9 eV. They suggest that the photoluminescence is associated with defect states at the etched surface. Shor et al. [221, 222] observed by cathodoluminescence a weak uv peak near 3.7 eV, beyond the bulk bad gap, in some samples of porous p-type 6H SiC. The origin of this peak has not been pinned down, and it has not been reported by other groups. Liao et al. [223 to 225] implanted Si with 50 keV carbon ions at fluences ranging from 10^{14} to $10^{17}\,\mathrm{cm}^{-2}$. After thermal annealing in N_2 at 950 to 1050 °C for 1 h and anodization in an HF–ethanol solution, they observed a blue band near 480 nm that increases with fluence and attributed it to a thin layer of porous 3C SiC. TEM and FTIR spectroscopy were used to provide evidence for the existence of a buried layer with 3C SiC. Van de Lagemaat et al. [220] observed an enhanced photocurrent in a SiC–electrolyte diode after the n-type 6H SiC was made porous.

The vibrational modes of small SiC particles have been studied by infrared and Raman spectroscopies for many years. A purpose of this work was to understand differences in the behavior of fine particles from the bulk material (e.g., surface polariton modes) and to test effective medium theories for the optical properties of mixtures of particles and supporting hosts. Englman and Ruppin [226] applied the theory of the absorption of electromagnetic radiation by small cylinders of polar material to explain the observation of an absorption mode at $941\,\mathrm{cm}^{-1}$ in 125 Å diameter 3C SiC fibers by Pultz and Hertl [227]. Ahn et al. [228] applied effective medium theory to the reststrahl bands observed in hot-pressed mixtures of SiC whiskers in Al_2O_3, taking into account the average over particle orientation. In their work, the Effective Medium Approximation [229] provided a superior description of the data over the Maxwell-Garnett model [230]. DiGregorio and Furtak [231] were able to interpret an additional mode beyond those observed in the bulk for irregular $\approx 3\,\mu\mathrm{m}$ average size 6H SiC particles as a surface polariton using the Maxwell-Garnett effective medium theory by setting the volume fraction of SiC particles in the calculation artificially high to take aggregation into account. Sasaki et al. [232] measured both infrared and Raman spectra of small SiC particles and analyzed the results using Mie theory and the Maxwell-Garnett model. Their primary interest was the size dependence of the phonons in small particles. Their coated sphere model for the particles includes a Drude component for free carriers in the interior surrounded by a carrier free shell modeled by a single oscillator alone.

MacMillan et al. [233, 234] recently studied the room temperature infrared reflectance of thick p-type porous 6H SiC layers. The reflectance in the reststrahl region is considerably modified. Fig. 8 shows that a portion of the region of high reflectance is lost, leaving a small reflectance peak near the longitudinal optic frequency ω_L. The region of reduced reflectance expands towards the transverse optic frequency ω_T with increasing porosity, which correlates with etch current density, and the peak near ω_L shrinks. A

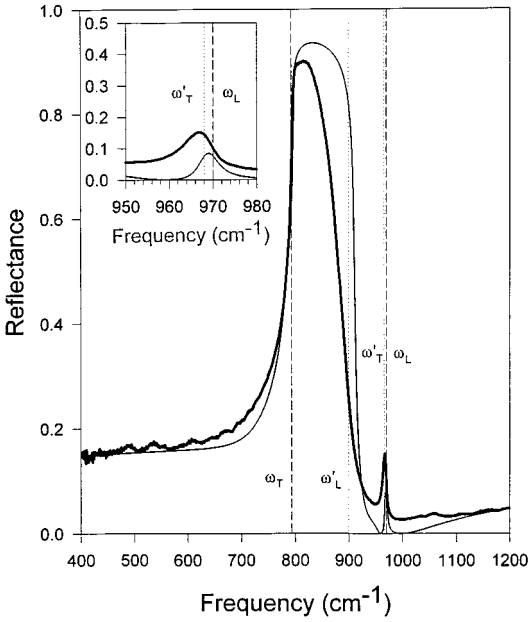

Fig. 8. Room temperature near normal incidence (5°) reflectance of a 128 μm thick porous 6H SiC layer on a 172 μm thick 6H SiC layer. Thick line: data; thin line: C-MG model. ω_T and ω_L are the transverse and longitudinal optic frequencies for a single Lorentz oscillator model of the dielectric function of 6H SiC in the reststrahl region. The frequencies ω'_T and ω'_L appear in the C-MG model ([234])

similar infrared spectrum was observed by Danishevskii et al. [219], who also performed Raman scattering on their samples. We interpreted this behavior using the Maxwell-Garnett effective medium theory [230]. This model is appropriate for an asymmetric microstructure, with one of the materials acting as a host and the other as inclusions. Unlike the studies of SiC particles discussed in the previous paragraph, we chose to treat the cavities as the inclusions imbedded in 6H SiC, a sensible description of the microstructure observed by transmission electron microscopy. The agreement between this Cavity-inclusion Maxwell-Garnett (C-MG) model and the data, shown in Fig. 8 for one sample, leads to an interpretation of the changes in the spectrum as due to polarization effects associated with the cavities combined with a mean field average of interactions among the cavities. Several other effective medium models based on alternative microstructures failed to describe the observed reflectance [234].

Acknowledgement We dedicate this article to Lyle Patrick, who passed away on Christmas Day, 1996. His many contributions to our knowledge of the optical properties of SiC form an essential part of the foundation for the recent progress we review here.

References

[1] W. J. Choyke, Mater. Res. Bull. **4**, 141 (1969).
[2] W. J. Choyke and L. Patrick, in: Silicon Carbide, Ed. R. C. Marshall, J. W. Faust, Jr., and C. E. Ryan, University of South Carolina Press, Columbia (SC) 1974 (p. 261).
[3] W. J. Choyke, Inst. Phys. Conf. Ser. No. 31, 58 (1977).
[4] W. J. Choyke, in: Proc. 20th Coll. Spectroscopicum Internationale and 7th Internat. Conf. Atomic Spectroscopy, Statni Pedagogické Nakladatelstvi, Praha 1977 (p. 385).
[5] W. J. Choyke, in: Mater. Res. Soc. Symp. Proc. **97**, 207 (1987).
[6] W. J. Choyke, NATO ASI Ser. **185**, 563 (1990).
[7] G. Pensl and W. J. Choyke, Physica **185B**, 264 (1993).
[8] W. J. Choyke and R. P. Devaty, Proc. 1st Europ. Conf. Silicon Carbide and Related Materials, ECSCRM'96, Heraklion, Crete (Greece), Oct. 6 to 9, 1996, Elsevier, Oxford, to be published.

[9] H. R. Phillip and E. A. Taft, in: Silicon Carbide – A High Temperature Semiconductor, Ed. J. R. O'Connor and J. Smiltens, Pergamon Press, Oxford 1960 (p. 366).
[10] B. E. Wheeler, Solid State Commun. **4**, 173 (1966).
[11] M. L. Belle, N. K. Prokofeva, and M. B. Reifman, Fiz. Tekh. Poluprov. **1**, 383 (1967) (Soviet Phys. – Semicond. **1**, 315 (1967)).
[12] V. Rehn, J. L. Stanford, V. O. Jones, and W. J. Choyke, Proc. 13th Internat. Conf. Physics of Semiconductors, Rome, 1976, Marves, Rome 1976 (p. 985).
[13] F. Herman, J. P. Van Dyke, and R. L. Kortum, Mater. Res. Bull. **4**, S167 (1969).
[14] L. A. Hemstreet, Jr., and C. Y. Fong, Solid State Commun. **9**, 643 (1971).
[15] L. A. Hemstreet. Jr., and C. Y. Fong, Phys. Rev. B **6**, 1464 (1972).
[16] L. A. Hemstreet and C. Y. Fong, in: Silicon Carbide, Ed. R. C. Marshall, J. W. Faust, Jr., and C. E. Ryan, University of South Carolina Press, Columbia (SC) 1974 (p. 284).
[17] V. V. Nemoshkalenko, V. G. Aleshin, M. T. Panchenko, and A. I. Senkevich, Dokl. Akad. Nauk SSSR **214**, 543 (1974) (Soviet Phys. – Doklady **19**, 38 (1974)).
[18] A. R. Lubinsky, D. E. Ellis, and G. S. Painter, Phys. Rev. B **11**, 1537 (1975).
[19] H.-G. Junginger and W. van Haeringen, phys. stat. sol. **37**, 709 (1970).
[20] W. R. L. Lambrecht, B. Segall, W. Suttrop, M. Yoganathan, R. P. Devaty, W. J. Choyke, J. A. Edmond, J. A. Powell, and M. Alouani, Appl. Phys. Lett. **63**, 2747 (1993).
[21] W. R. L. Lambrecht, B. Segall, M. Yoganathan, W. Suttrop, R. P. Devaty, W. J. Choyke, J. A. Edmond, J. A. Powell, and M. Alouani, Phys. Rev. B **50**, 10,722 (1994).
[22] W. Suttrop, M. Yoganathan, R. P. Devaty, W. J. Choyke, J. A. Edmond, J. A. Powell, W. R. L. Lambrecht, B. Segall, and M. Alouani, Inst. Phys. Conf. Ser. No. 137, 169 (1993).
[23] W. J. Choyke and L. Patrick, J. Opt. Soc. Amer. **58**, 377 (1968).
[24] S. Logothetidis, H. M. Polatoglou, J. Petalas, D. Fuch, and R. L. Johnson, Physica **185 B**, 389 (1993).
[25] S. Logothetidis and J. Petalas, J. Appl. Phys. **80**, 1768 (1996).
[26] B. Adolph, V. Gavrilenko, K. Tenelsen, and F. Bechstedt, Inst. Phys. Conf. Ser. No. 142, 305 (1996).
[27] B. Adolph, V. Gavrilenko, K. Tenelsen, F. Bechstedt, and R. Del Sole, Phys. Rev. B **53**, 9797 (1996).
[28] V. I. Gavrilenko and F. Bechstedt, Phys. Rev. B **54**, 13,416 (1996).
[29] B. Wenzien, P. Käckell, F. Bechstedt, and G. Cappellini, Phys. Rev. B **52**, 10,897 (1995).
[30] M. Rohlfing, P. Krüger, and J. Pollmann, Phys. Rev. B **48**, 17,791 (1993).
[31] W. H. Backes, P. A. Bobbert, and W. van Haeringen, Phys. Rev. B **51**, 4950 (1995).
[32] W. R. L. Lambrecht, S. Limpijumnong, S. Rashkeev, and B. Segall, phys. stat. sol. (b) **202**, 5 (1997).
[33] V. I. Gavrilenko, S. I. Frolov, and N. I. Klyui, Physica **185 B**, 394 (1993).
[34] V. I. Gavrilenko, A. V. Postnikov, N. I. Klyui, and V. G. Litovchenko, phys. stat. sol. (b) **162**, 477 (1990).
[35] V. I. Gavrilenko, Appl. Phys. Lett. **67**, 16 (1995).
[36] B. Adolph, K. Tenelsen, V. I. Gavrilenko, and F. Bechstedt, Phys. Rev. B **55**, 1422 (1997).
[37] R. S. Knox, Theory of Excitons, Solid State Physics, Suppl. 5, Academic Press, New York 1963.
[38] J. O. Dimmock, in: Semiconductors and Semimetals, Vol. 3, Ed. R. K. Willardson and A. C. Beer, Academic Press, New York 1967 (pp. 259 to 319).
[39] D. C. Reynolds and T. C. Collins, Excitons: Their Properties and Uses, Academic Press, New York 1981.
[40] D. Labrie, M. L. W. Thewalt, I. J. Booth, and G. Kirczenow, Phys. Rev. Lett. **61**, 1882 (1988).
[41] T. P. McLean and R. Loudon, J. Phys. Chem. Solids **13**, 1 (1960).
[42] N. O. Lipari and M. Altarelli, Solid State Commun. **18**, 951 (1976).
[43] N. O. Lipari and M. Altarelli, Phys. Rev. B **15**, 4883 (1977).
[44] D. Bimberg, M. Altarelli, and N. O. Lipari, Solid State Commun. **40**, 437 (1981).

[45] R. J. Elliott and R. Loudon, J. Phys. Chem. Solids **15**, 146 (1960).
[46] M. Lax and J. J. Hopfield, Phys. Rev. **124**, 115 (1961).
[47] I. S. Gorban, V. A. Gubanov, V. G. Lysenko, A. A. Pletyushkin, and V. B. Timofeev, Fiz. Tverd. Tela **26**, 2282 (1984) (Soviet Phys. – Solid State **26**, 1385 (1984)).
[48] Yu. A. Vakulenko, I. S. Gorban, V. A. Gubanov, and A. A. Pletyushkin, Fiz. Tverd. Tela **26**, 3555 (1984) (Soviet Phys. – Solid State **26**, 2139 (1984)).
[49] V. I. Sankin, Fiz. Tverd. Tela **15**, 961 (1973) (Soviet Phys. – Solid State **15**, 671 (1973)).
[50] D. Bimberg, M. S. Skolnick, and W. J. Choyke, Phys. Rev. Lett. **40**, 56 (1978).
[51] D. Bimberg, L. M. Sander, M. S. Skolnick, U. Rössler, and W. J. Choyke, J. Lum. **18/19**, 542 (1979).
[52] M. S. Skolnick, D. Bimberg, and W. J. Choyke, Solid State Commun. **28**, 865 (1978).
[53] R. J. Elliott, Phys. Rev. **108**, 1384 (1957).
[54] W. J. Choyke and L. Patrick, Phys. Rev. **127**, 1868 (1962).
[55] L. Patrick, W. J. Choyke, and D. R. Hamilton, Phys. Rev. **137**, A1515 (1965).
[56] W. J. Choyke, D. R. Hamilton, and L. Patrick, Phys. Rev. **133**, A1163 (1964).
[57] L. Patrick, D. R. Hamilton, and W. J. Choyke, Phys. Rev. **132**, 2023 (1963).
[58] D. R. Hamilton, L. Patrick, and W. J. Choyke, Phys. Rev. **138**, A1472 (1965).
[59] W. J. Choyke, D. R. Hamilton, and L. Patrick, Phys. Rev. **139**, A1262 (1965).
[60] L. Patrick, D. R. Hamilton, and W. J. Choyke, Phys. Rev. **143**, 526 (1966).
[61] D. S. Nedzvetskii, B. V. Novikov, N. K. Prokofeva, and M. B. Reifman, Fiz. Tekh. Poluprov. **2**, 1089 (1968) (Soviet Phys. – Semicond. **2**, 914 (1968)).
[62] A. N. Pikhtin and D. A. Yaskov, Fiz. Tverd. Tela **12**, 1597 (1970) (Soviet Phys. – Solid State **12**, 1267 (1970)).
[63] M. Cardona, Modulation Spectroscopy, Solid State Physics, Suppl. 11, Academic Press, New York 1969.
[64] C. Persson and U. Lindefelt, Phys. Rev. B **54**, 10,257 (1996).
[64a] G. Wellenhofer and U. Rössler, phys. stat. sol. (b) **202**, 107 (1997).
[65] G. B. Dubrovskii and V. I. Sankin, Fiz. Tverd. Tela **14**, 1200 (1972) (Soviet Phys. – Solid State **14**, 1024 (1972)).
[66] V. I. Sankin, Fiz. Tverd. Tela **17**, 1820 (1975) (Soviet Phys. – Solid State **17**, 1191 (1975)).
[67] G. B. Dubrovskii and V. I. Sankin, Fiz. Tverd. Tela **17**, 1847 (1975) (Soviet Phys. – Solid State **17**, 1847 (1975)).
[68] R. G. Humphreys, D. Bimberg, and W. J. Choyke, J. Phys. Soc. Japan **49**, Suppl. A, 519 (1980).
[69] R. G. Humphreys, D. Bimberg, and W. J. Choyke, Solid State Commun. **39**, 163 (1981).
[70] V. A. Kiselev, B. V. Novikov, M. M. Pimonenko, and E. B. Shadrin, Fiz. Tverd. Tela **13**, 1118 (1971) (Soviet Phys. – Solid State **13**, 926 (1971)).
[71] M. Ikeda and H. Matsunami, phys. stat. sol. (a) **58**, 657 (1980).
[72] O. Kordina, A. Henry, C. Hallin, R. C. Glass, A. O. Konstantinov, C. Hemmingsson, N. T. Son, and E. Janzén, Mater. Res. Soc. Symp. Proc. **339**, 405 (1994).
[73] O. Kordina, C. Hallin, A. Ellison, A. S. Bakin, I. G. Ivanov, A. Henry, R. Yakimovà, M. Touminen, A. Vehanen, and E. Janzén, Appl. Phys. Lett. **69**, 1456 (1996).
[74] O. Kordina, A. Henry, J. P. Bergman, N. T. Son, W. M. Chen, C. Hallin, and E. Janzén, Appl. Phys. Lett. **66**, 1373 (1995).
[75] L. L. Clemen, R. P. Devaty, M. F. Mac Millan, W. J. Choyke, A. A. Burk, Jr., D. L. Barrett, H. M. Hobgood, D. J. Larkin, and J. A. Powell, Inst. Phys. Conf. Ser. No. 137, 147 (1994).
[76] J. M. Luttinger and W. Kohn, Phys. Rev. **97**, 869 (1955).
[77] W. Kohn, Solid State Physics, Vol. 5, Ed. F. Seitz and D. Turnbull, Academic Press, New York 1957 (pp. 257 to 320).
[78] A. K. Ramdas and S. Rodriguez, Rep. Progr. Phys. **44**, 1297 (1981).
[79] L. Patrick and W. J. Choyke, Phys. Rev. B **2**, 2255 (1970).
[80] W. J. Moore, R. T. Holm, M. J. Yang, and J. A. Freitas, Jr., J. Appl. Phys. **78**, 7255 (1995).
[81] K. Karch, F. Bechstedt, P. Pavone, and D. Strauch, Phys. Rev. B **53**, 13,400 (1996).
[82] K. Karch, F. Bechstedt, P. Pavone, and D. Strauch, J. Phys.: Condensed Matter **8**, 2945 (1996).

[83] D. Volm, B. K. Meyer, D. M. Hofmann, W. M. Chen, N. T. Son, C. Persson, U. Lindefelt, O. Kordina, E. Sörman, A. O. Konstantinov, B. Monemar, and E. Janzén, Phys. Rev. B **53**, 15,409 (1996).
[84] W. R. L. Lambrecht and B. Segall, Phys. Rev. B **52**, R2249 (1995).
[85] P. Srichaikul and A.-B. Chen, Inst. Phys. Conf. Ser. No. 142, 285 (1995).
[86] G. Wellenhofer and U. Rössler, Solid State Commun. **96**, 887 (1995).
[87] P. J. Dean, W. J. Choyke, and L. Patrick, J. Lum. **15**, 299 (1977).
[88] R. Kaplan, R. J. Wagner, H. J. Kim, and R. F. Davis, Solid State Commun. **55**, 67 (1985).
[89] W. J. Moore, P. J. Lin-Chung, J. A. Freitas, Jr., Yu. M. Altaiskii, V. L. Zuev, and L. M. Ivanova, Phys. Rev. B **48**, 12,289 (1993).
[90] W. J. Moore, J. A. Freitas, Jr., Yu. M. Altaiskii, V. L. Zuev, and L. M. Ivanova, Inst. Phys. Conf. Ser. No. 137, 181 (1993).
[91] W. J. Moore, J. A. Freitas, Jr., and P. J. Lin-Chung, Solid State Commun. **93**, 389 (1995).
[92] J. Kono, S. Takeyama, H. Yokoi, N. Miura, M. Yamanaka, M. Shinohara, and K. Ikoma, Phys. Rev. B **48**, 10,909 (1993).
[93] S. Takeyama, J. Kono, N. Miura, M. Yamanaka, M. Shinohara, and K. Ikoma, Physica **185B**, 384 (1993).
[94] J. Kono, N. Miura, S. Takeyama, H. Yokoi, N. Fujimori, Y. Nishibayashi, T. Nakajima, K. Tsuji, and M. Yamanaka, Physica **184B**, 178 (1993).
[95] N. T. Son, W. M. Chen, O. Kordina, A. O. Konstantinov, B. Monemar, E. Janzén, D. M. Hofmann, D. Volm, M. Drechsler, and B. K. Meyer, Appl. Phys. Lett. **66**, 1074 (1995).
[96] N. T. Son, O. Kordina, A. O. Konstantinov, W. M. Chen, E. Sörman, B. Monemar, and E. Janzén, Appl. Phys. Lett. **65**, 3209 (1994).
[97] L. Patrick, Phys. Rev. B **5**, 2198 (1972).
[98] D. J. Larkin, P. G. Neudeck, J. A. Powell, and L. G. Matus, Appl. Phys. Lett. **65**, 1659 (1994).
[99] D. J. Larkin, P. G. Neudeck, J. A. Powell, and L. G. Matus, Inst. Phys. Conf. Ser. No. 137, 51 (1994).
[100] D. J. Larkin, Inst. Phys. Conf. Ser. No. 142, 23 (1996).
[101] T. N. Morgan, Phys. Rev. Lett. **21**, 819 (1968).
[102] E. Biedermann, Solid State Commun. **3**, 343 (1965).
[103] G. B. Dubrovskii, A. A. Lepneva, and E. I. Radovanova, phys. stat. sol. (b) **57**, 423 (1973).
[104] I. S. Gorban, A. P. Krokhmal, V. I. Levin, A. S. Skirda, Yu. M. Tairov, and V. F. Tsvetkov, Fiz. Tekh. Poluprov. **21**, 194 (1987) (Soviet Phys. – Semicond. **21**, 119 (1987)).
[105] M. Ikeda, H. Matsunami, and T. Tanaka, Phys. Rev. B **22**, 2842 (1980).
[106] M. A. Lampert, Phys. Rev. Lett. **1**, 450 (1958).
[107] M. Hofmann, A. Zywietz, K. Karch, and F. Bechstedt, Phys. Rev. B **50**, 13,401 (1994).
[108] W. R. L. Lambrecht, S. Limpijumnong, and B. Segall, Inst. Phys. Conf. Ser. No. 142, 263 (1996).
[109] W. J. Choyke, R. P. Devaty, L. L. Clemen, M. F. MacMillan, M. Yoganathan, and G. Pensl, Inst. Phys. Conf. Ser. No. 142, 257 (1996).
[110] R. L. Hartman and P. J. Dean, Phys. Rev. B **2**, 951 (1970).
[111] D. G. Thomas, M. Gershenzon, and J. J. Hopfield, Phys. Rev. **131**, 2397 (1963).
[112] P. J. Dean and R. L. Hartman, Phys. Rev. B **5**, 4911 (1972).
[113] C. Wecker, M. Certier, S. Nikitine, and L. Dietrich, phys. stat. sol. (b) **50**, K81 (1972).
[114] I. S. Gorban, A. P. Krokhmal, and I. A. Rozhko, Fiz. Tverd. Tela **31**, 126 (1989) (Soviet Phys. – Solid State **31**, 2095 (1989)).
[115] Ch. Haberstroh, R. Helbig, and R. A. Stein, J. Appl. Phys. **76**, 509 (1994).
[116] M. Kobayashi, M. Yamanaka, and M. Shinohara, J. Phys. Soc. Japan **58**, 2673 (1989).
[117] P. E. Van Camp, V. E. Van Doren, and J. T. Devreese, phys. stat. sol. (b) **146**, 573 (1988).
[118] K. J. Chang and M. L. Cohen, Phys. Rev. B **35**, 8196 (1987).

[119] C. H. Park, B. H. Cheong, K. H. Lee, and K. J. Chang, Phys. Rev. B **49**, 4485 (1994).
[120] K. Karch, F. Bechstedt, P. Pavone, and D. Strauch, J. Phys.: Condens. Matter **8**, 2945 (1996).
[121] F. Engelbrecht, J. Zeman, G. Wellenhofer, C. Peppermüller, R. Helbig, G. Martinez, and U. Rössler, phys. stat. sol. (b) **198**, 81 (1996).
[122] J. R. Haynes, Phys. Rev. Lett. **4**, 361 (1960).
[123] P. J. Dean, R. A. Faulkner, S. Kimura, and M. Ilegems, Phys. Rev. B **4**, 1926 (1971).
[124] P. J. Dean and D. C. Herbert, in: Excitons, Topics in Current Physics, Vol. 14, Ed. K. Cho, Springer-Verlag, Berlin 1979 (pp. 55 to 182).
[125] J. L. Merz, H. Kukimoto, K. Nassau, and J. W. Shiever, Phys. Rev. B **6**, 545 (1972).
[126] R. A. Faulkner, Phys. Rev. **184**, 713 (1969).
[127] P. J. Dean, D. C. Herbert, D. Bimberg, and W. J. Choyke, Phys. Rev. Lett. **37**, 1635 (1976).
[128] D. C. Herbert, P. J. Dean, and W. J. Choyke, Solid State Commun. **24**, 383 (1977).
[129] V. D. Kulakovskii and V. A. Gubanov, Zh. Eksper. Teor. Fiz. **88**, 937 (1985) (Soviet Phys. – J. Exper. Theor. Phys. **61**, 550 (1985)).
[130] V. D. Kulakovskii and V. A. Gubanov, Fiz. Tverd. Tela **27**, 2264 (1985) (Soviet Phys. – Solid State **27**, 1359 (1985)).
[131] G. Kirczenow, Canad. J. Phys. **55**, 1787 (1977).
[132] L. L. Clemen, M. Yoganathan, W. J. Choyke, R. P. Devaty, H. S. Kong, J. A. Edmond, D. J. Larkin, J. A. Powell, and A. A. Burk, Jr., Inst. Phys. Conf. Ser. No. 137, 251 (1994).
[133] A. Henry, O. Kordina, C. Hallin, C. Hemmingsson, and E. Janzén, Appl. Phys. Lett. **65**, 2457 (1994).
[134] I. G. Ivanov, C. Hallin, A. Henry, O. Kordina, and E. Janzén, J. Appl. Phys. **80**, 3504 (1996).
[135] P. A. Gaubis, PhD Thesis, Michigan State University, 1977 (University Microfilms International, Ann Arbor, MI), #78-10053.
[136] Yu. A. Vakulenko, I. S. Gorban', V. A. Gubanov, and A. A. Pletyushkin, Fiz. Tverd. Tela **27**, 282 (1985) (Soviet Phys. – Solid State **27**, 173 (1985)).
[137] W. Suttrop, G. Pensl, W. J. Choyke, R. Stein, and S. Leibenzeder, J. Appl. Phys. **72**, 3708 (1992).
[138] W. Götz, A. Schöner, G. Pensl, W. Suttrop, W. J. Choyke, R. Stein, and S. Leibenzeder, J. Appl. Phys. **73**, 3332 (1993).
[139] Th. Troffer, W. Götz, A. Schöner, W. Suttrop, G. Pensl, R. P. Devaty, and W. J. Choyke, Inst. Phys. Conf. Ser. No. 137, 173 (1994).
[140] G. B. Dubrovskii and E. I. Radovanova, phys. stat. sol. (b) **48**, 875 (1971).
[141] O. V. Vakulenko and O. A. Guseva, Fiz. Tekh. Poluprov. **15**, 1528 (1981) (Soviet Phys. – Semicond. **15**, 886 (1981)).
[142] W. Götz, A. Schöner, W. Suttrop, G. Pensl, W. J. Choyke, R. A. Stein, and S. Leibenzeder, Mater. Sci. Forum **143** to **147**, 69 (1994).
[143] F. Engelbrecht and R. Helbig, Mater. Res. Soc. Symp. Proc. **339**, 529 (1994).
[144] F. Engelbrecht, S. Huant, and R. Helbig, Phys. Rev. B **52**, 11,008 (1995).
[145] P. Srichaikul, PhD Thesis, Auburn University, 1995 (unpublished).
[146] A.-B. Chen and P. Srichaikul, phys. stat. sol. (b) **202**, 81 (1997).
[147] A. I. Veinger, A. G. Zabrodskii, G. A. Lomakina, and E. N. Mokhov, Fiz. Tverd. Tela **28**, 1659 (1986) (Soviet Phys. – Solid State **28**, 917 (1986)).
[148] E. N. Kalabukhova, S. N. Lukhin, and E. N. Mokhov, Fiz. Tverd. Tela **35**, 703 (1993) (Soviet Phys. – Solid State **35**, 361 (1993)).
[149] E. N. Kalabukhova, S. N. Lukin, E. N. Mokhov, M. Feege, S. Greulich-Weber, and J.-M. Spaeth, Inst. Phys. Conf. Ser. No. 137, 215 (1994).
[150] S. Greulich-Weber, M. Feege, J.-M. Spaeth, E. N. Kalabukhova, S. N. Lukin, and E. N. Mokhov, Solid State Commun. **93**, 393 (1995).
[151] H. Sonntag and S. Kalbitzer, Appl. Phys. A **61**, 363 (1995).
[152] T. Troffer, C. Peppermüller, G. Pensl, K. Rottner, and A. Schöner, J. Appl. Phys. **80**, 3739 (1996).

[153] L. L. Clemen, S. G. Sridhara, D. G. Nizhner, R. P. Devaty, W. J. Choyke, D. J. Larkin, and G. Pensl, to be published.
[154] G. F. Koster, Solid State Phys. **5**, 173 (1957).
[155] D. G. Thomas and J. J. Hopfield, Phys. Rev. **128**, 2135 (1962).
[156] J. J. Hopfield, J. Phys. Chem. Solids **15**, 97 (1960).
[157] G. L. Bir and G. E. Pikus, Symmetry and Strain-Induced Effects in Semiconductors, Wiley, New York 1974.
[158] A. K. Ramdas and S. Rodriguez, Rep. Progr. Phys. **44**, 1297 (1981).
[159] L. L. Clemen, W. J. Choyke, R. P. Devaty, J. A. Powell, and H. S. Kong, in: Amorphous and Crystalline Silicon Carbide IV, Ed. C. Y. Yang, M. M. Rahman, and G. L. Harris, Proceedings in Physics, Vol. 71, Springer-Verlag, Berlin 1992 (p. 105).
[160] L. L. Clemen, R. P. Devaty, M. F. MacMillan, M. Yoganathan, W. J. Choyke, D. J. Larkin, J. A. Powell, J. A. Edmond, and H. S. Kong, Appl. Phys. Lett. **62**, 2953 (1993).
[161] L. L. Clemen, R. P. Devaty, W. J. Choyke, J. A. Powell, D. J. Larkin, J. A. Edmond, and A. A. Burk, Jr., Inst. Phys. Conf. Ser. No. 137, 297 (1994).
[162] P. J. Dean, R. A. Faulkner, and S. Kimura, Phys. Rev. B **2**, 4062 (1970).
[163] S. V. Bogdanov and V. A. Gubanov, Fiz. Tekh. Poluprov. **22**, 728 (1988) (Soviet Phys. – Semicond. **22**, 453 (1988)).
[164] L. L. Clemen, PhD Thesis, University of Pittsburgh, 1994 (unpublished).
[165] L. S. Dang, K. M. Lee, G. D. Watkins, and W. J. Choyke, Phys. Rev. Lett. **45**, 390 (1980).
[166] A. Henry, C. Hallin, I. G. Ivanov, J. P. Bergman, O. Kordina, and E. Janzén, Inst. Phys. Conf. Ser. No. 142, 381 (1996).
[167] A. Henry, C. Hallin, I. G. Ivanov, J. P. Bergman, O. Kordina, U. Lindefelt, and E. Janzén, Phys. Rev. B **53**, 13503 (1996).
[168] K. Colbow, Phys. Rev. **141**, 742 (1966).
[169] R. Z. Bachrach and O. G. Lorimor, Phys. Rev. B **7**, 700 (1973).
[170] M. Ikeda, H. Matsunami, and T. Tanaka, J. Lum. **20**, 111 (1979).
[171] M. Yoganathan, W. J. Choyke, R. P. Devaty, and P. G. Neudeck, J. Appl. Phys. **80**, 1763 (1996).
[172] P. J. Dean, Progr. Solid State Chem. **8**, 1 (1973).
[173] J. J. Hopfield, D. G. Thomas, and M. Gershenzon, Phys. Rev. Lett. **10**, 162 (1963).
[174] C. H. Henry, R. A. Faulkner, and K. Nassau, Phys. Rev. **183**, 798 (1969).
[175] J. D. Wiley and J. A. Seman, Bell Syst. Tech. J. **49**, 355 (1970).
[176] L. Patrick, Phys. Rev. **180**, 794 (1969).
[177] W. J. Choyke and L. Patrick, Phys. Rev. B **2**, 4959 (1970).
[178] H. Kuwabara, K. Yamanaka, and S. Yamada, phys. stat. sol. (a) **37**, K157 (1976).
[179] G. Zanmarchi, J. Phys. Chem. Solids **29**, 1727 (1968).
[180] T. N. Morgan, Phys. Rev. Lett. **24**, 887 (1970).
[181] J. F. Scott, D. J. Toms, and W. J. Choyke, Phys. Rev. B **21**, 3432 (1980).
[182] J. F. Scott, D. J. Toms, L. S. Dang, K. M. Lee, G. D. Watkins, and W. J. Choyke, Phys. Rev. B **23**, 2029 (1981).
[183] J. Reinke, S. Greulich-Weber, and J.-M. Spaeth, Solid State Commun. **98**, 835 (1996).
[184] P. G. Baranov, V. A. Vetrov, N. G. Romanov, and V. I. Sokolov, Fiz. Tverd. Tela **27**, 3459 (1985) (Soviet Phys. – Solid State **27**, 2085 (1985)).
[185] G. A. Lomakina, Fiz. Tverd. Tela **7**, 600 (1965) (Soviet Phys. – Solid State **7**, 475 (1965)).
[186] J. M. Blank, Mater. Res. Bull. **4**, S179 (1969).
[187] S. Yamada and H. Kuwabara, in: Silicon Carbide 1973, University of South Carolina Press, Columbia (SC) 1974 (p. 305).
[188] H. Kuwabara and S. Yamada, phys. stat. sol. (a) **30**, 739 (1975).
[189] S. G. Sridhara, L. L. Clemen, D. G. Nizhner, R. P. Devaty, W. J. Choyke, D. Larkin, H. S. Kong, T. Troffer, and G. Pensl, unpublished.
[190] D. J. Larkin, S. G. Sridhara, R. P. Devaty, and W. J. Choyke, J. Electronic Mater. **24**, 289 (1995).
[191] L. Patrick and W. J. Choyke, Phys. Rev. B **9**, 1997 (1974).
[192] W. J. Choyke, P. J. Dean, and L. Patrick, Phys. Rev. B **10**, 2554 (1974).

[193] L. L. Clemen, R. P. Devaty, W. J. Choyke, A. A. Burk, Jr., D. J. Larkin, and J. A. Powell, Inst. Phys. Conf. Ser. No. 137, 227 (1993).
[194] G. S. Pomrenke, P. B. Klein, and D. W. Langer, Mater. Res. Soc. Symp. Proc. **301** (1993).
[195] S. Coffa, A. Polman, and R. N. Schwartz, Mater. Res. Soc. Symp. Proc. **422** (1996).
[196] G. H. Dieke, Spectra and Energy Levels of Rare Earth Ions in Crystals, Wiley, New York 1968.
[197] S. Hüfner, Optical Spectra of Transparent Rare Earth Compounds, Academic Press, New York 1978.
[198] B. R. Judd, Phys. Rev. **127**, 750 (1962).
[199] G. S. Ofelt, J. Chem. Phys. **37**, 511 (1962).
[200] K. R. Lea, M. J. M. Leask, and W. P. Wolf, J. Phys. Chem. Solids **23**, 1381 (1962).
[201] W. J. Choyke, R. P. Devaty, L. L. Clemen, M. Yoganathan, G. Pensl, and Ch. Hässler, Appl. Phys. Lett. **65**, 1668 (1994).
[202] M. Yoganathan, W. J. Choyke, R. P. Devaty, G. Pensl, and J. A. Edmond, Mater. Res. Soc. Symp. Proc. **422**, 39 (1996).
[203] W. J. Choyke, R. P. Devaty, M. Yoganathan, G. Pensl, and J. A. Edmond, Proc. 7th Internat. Conf. Shallow-Level Centers in Semiconductors, World Scientific Publ. Co., Singapore, to be published in March, 1997.
[204] W. J. Choyke, R. P. Devaty, L. L. Clemen, M. F. MacMillan, M. Yoganathan, and G. Pensl, Inst. Phys. Conf. Ser. No. 142, 257 (1996).
[205] M. Yoganathan, W. J. Choyke, R. P. Devaty, G. Pensl, and J. A. Edmond, Inst. Phys. Conf. Proc. No. 142, 377 (1996).
[206] P. Galtier, T. Benyattou, J. P. Pocholle, M. N. Charasse, G. Guillot, and J. P. Hirtz, Inst. Phys. Conf. Ser. No. 106, 327 (1989).
[207] M. Yoganathan, PhD Thesis, University of Pittsburgh, 1996 (unpublished).
[208] A. J. Steckl, J. Devrajan, W. J. Choyke, R. P. Devaty, M. Yoganathan, and S. W. Novak, J. Electronic Mater. **25**, 869 (1996).
[209] J. S. Shor, I. Grimberg, B. Z. Weiss, and A. D. Kurtz, Appl. Phys. Lett. **62**, 2836 (1993).
[210] A. Takazawa, A. Tamura, and Y. Yamada, Japan. J. Appl. Phys. **32**, 3148 (1993).
[211] C. I. Harris, R. Glass, O. Kordina, M. Syväjärvi, and E. Janzén, Inst. Phys. Conf. Ser. No. 137, 617 (1993).
[212] T. Matsumoto, T. Tamaki, T. Futagi, H. Mimura, and Y. Kanemitsu, Mater. Res. Soc. Symp. Proc. **298**, 355 (1993).
[213] T. Matsumoto, J. Takahashi, T. Tamaki, T. Fugati, and H. Mimura, Appl. Phys. Lett. **64**, 226 (1994).
[214] H. Mimura, T. Matsumoto, and Y. Kanemitsu, Appl. Phys. Lett. **65**, 3350 (1994).
[215] A. O. Konstantinov, C. I. Harris, and E. Janzén, Appl. Phys. Lett. **65**, 2699 (1994).
[216] A. O. Konstantinov, A. Henry, C. I. Harris, and E. Janzén, Appl. Phys. Lett. **66**, 2250 (1995).
[217] A. O. Konstantinov, C. I. Harris, A. Henry, and E. Janzén, Inst. Phys. Conf. Ser. No. 142, 1079 (1995).
[218] W. Shin, K. Ishida, W.-S. Seo, Y. Suzuki, and K. Kuomoto, Inst. Phys. Conf. Ser. No. 142, 1071 (1995).
[219] A. M. Danishevskii, V. B. Shuman, A. Yu. Rogachev, and P. A. Ivanov, Semiconductors **29**, 1106 (1995).
[220] J. van de Lagemaat, M. Plakman, D. Vanmaekelbergh, and J. J. Kelly, Appl. Phys. Lett. **69**, 2246 (1996).
[221] J. S. Shor, L. Bemis, A. D. Kurtz, M. F. MacMillan, W. J. Choyke, I. Grimberg, and B. Z. Weiss, Inst. Phys. Conf. Ser. No. 137, 193 (1993).
[222] J. S. Shor, L. Bemis, A. D. Kurtz, I. Grimberg, B. Z. Weiss, M. F. MacMillan, and W. J. Choyke, J. Appl. Phys. **76**, 4045 (1994).
[223] L.-S. Liao, X.-M. Bao, Z.-F. Yang, and N.-B. Min, Appl. Phys. Lett. **66**, 2382 (1995).
[224] L.-S. Liao, X.-M. Bao, N.-S. Li, Z.-F. Yang, and N.-B. Min, Solid State Commun. **95**, 559 (1995).
[225] X.-M. Bao, L.-S. Liao, N.-S. Li, N.-B. Min, Y.-H. Gao, and Z. Zhang, Nuclear Instrum. and Methods B **119**, 505 (1996).

[226] R. Englman and R. Ruppin, J. Phys. C **1**, 1515 (1968).
[227] W. W. Pultz and W. Hertl, Spectrochim. Acta **22**, 573 (1966).
[228] J. S. Ahn, K. H. Kim, T. W. Noh, D.-H. Rin, K.-H. Boo, and H.-E. Kim, Phys. Rev. B **52**, 15244 (1995).
[229] D. Stroud, Phys. Rev. B **12**, 3368 (1975).
[230] J. C. M. Garnett, Philos. Trans. R. Soc. London, Ser. A **203**, 385 (1904); **205**, 237 (1906).
[231] J. F. DiGregorio and T. E. Furtak, Solid State Commun. **89**, 163 (1994).
[232] Y. Sasaki, Y. Nishina, M. Sato, and K. Okamura, Phys. Rev. B **40**, 1762 (1989).
[233] M. F. MacMillan, R. P. Devaty, W. J. Choyke, D. R. Goldstein, J. E. Spanier, and A. D. Kurtz, Inst. Phys. Conf. Ser. No. 142, 1075 (1996).
[234] M. F. MacMillan, R. P. Devaty, W. J. Choyke, D. R. Goldstein, J. E. Spanier, and A. D. Kurtz, J. Appl. Phys. **80**, 2412 (1996).